CART neurons in the arcuate nucleus and lateral hypothalamic area exert differential controls on energy homeostasis

Jackie Lau [1], Aitak Farzi [1,3], Yue Qi [1], Regine Heilbronn [2], Mario Mietzsch [2,4], Yan-Chuan Shi [1,**,5], Herbert Herzog [1,*,5]

ABSTRACT

Objective: The cocaine- and amphetamine-regulated transcript (CART) codes for a pivotal neuropeptide important in the control of appetite and energy homeostasis. However, limited understanding exists for the defined effector sites underlying CART function, as discrepant effects of central CART administration have been reported.

Methods: By combining *Cart-cre* knock-in mice with a *Cart* adeno-associated viral vector designed using the flip-excision switch (AAV-FLEX) technology, specific reintroduction or overexpression of CART selectively in CART neurons in the arcuate nucleus (Arc) and lateral hypothalamic area (LHA), respectively, was achieved. The effects on energy homeostasis control were investigated.

Results: Here we show that CART neuron-specific reintroduction of CART into the Arc and LHA leads to distinct effects on energy homeostasis control. Specifically, CART reintroduction into the Arc of otherwise CART-deficient *Cart$^{cre/cre}$* mice markedly decreased fat mass and body weight, whereas CART reintroduction into the LHA caused significant fat mass gain and lean mass loss, but overall unaltered body weight. The reduced adiposity in Arc^{CART};*Cart$^{cre/cre}$* mice was associated with an increase in both energy expenditure and physical activity, along with significantly decreased *Npy* mRNA levels in the Arc but with no change in food consumption. Distinctively, the elevated fat mass in LHA^{CART};*Cart$^{cre/cre}$* mice was accompanied by diminished insulin responsiveness and glucose tolerance, greater spontaneous food intake, and reduced energy expenditure, which is consistent with the observed decrease of brown adipose tissue temperature. This is also in line with significantly reduced tyrosine hydroxylase (*Th*) and notably increased corticotropin-releasing hormone (*Crh*) mRNA expressions in the paraventricular nucleus (PVN).

Conclusions: Taken together, these results identify catabolic and anabolic effects of CART in the Arc and LHA, respectively, demonstrating for the first time the distinct and region-specific functions of CART in controlling feeding and energy homeostasis.

© 2017 The Authors. Published by Elsevier GmbH. This is an open access article under the CC BY-NC-ND license (http://creativecommons.org/licenses/by-nc-nd/4.0/).

Keywords CART; Energy homeostasis; AAV-FLEX; Arcuate nucleus; Lateral hypothalamic area

1. INTRODUCTION

The cocaine- and amphetamine-regulated transcript (CART) is a major neuropeptide involved in the regulation of diverse biological processes, including appetite control, maintenance of body weight, reward and addiction, psychostimulant effects, and neuroendocrine functions [1]. Among the wide and abundant central distribution of the peptide associated with multiple neurocircuitries in mammals [2—4], CART expression shows predominance in neuroendocrine neurons [5], particularly in the hypothalamus at feeding-related regions [6,7]. Extensive research has focused on the role of CART in modulating feeding behavior and energy homeostasis [1], thereby exploring therapeutic potentials in the treatment of obesity and other metabolic disorders. However, identification of the hypothalamic sites of action and the mechanisms underlying CART function in homeostatic regulation remains challenging, mainly owing to the lack of information on the elusive CART receptor(s) that remain(s) unidentified [1]. In addition to the ubiquitous expression and broad connection of the peptide with various neuronal networks, the biosynthesis of CART involves complex post-translational processing, including the formation of various disulfide bonds [5,8], further rendering pharmacological intervention using any synthetic *ex-vivo* produced CART analogs difficult.

[1]Neuroscience Division, Garvan Institute of Medical Research, St. Vincent's Hospital, Darlinghurst, NSW 2010, Sydney, Australia [2]Charité - Universitätsmedizin Berlin, Corporate Member of Freie Universität Berlin, Humboldt-Universität zu Berlin, and Berlin Institute of Health, Institute of Virology, Campus Benjamin Franklin, Germany

[3] Present address: Institute of Experimental and Clinical Pharmacology, Medical University of Graz, Graz, AUSTRIA.
[4] Present address: Department of Biochemistry & Molecular Biology, Center for Structural Biology, The McKnight Brain Institute, University of Florida, Gainesville, FL 32610, USA.
[5] Contributed equally to this work.

*Corresponding author. E-mail: h.herzog@garvan.org.au (H. Herzog).

**Corresponding author. E-mail: y.shi@garvan.org.au (Y.-C. Shi).

The functional importance of CART is highlighted by the strong evolutionary conservation across species [1,9]. Moreover, CART expression patterns are very similar between rodents and human, with high density of expression in hypothalamic areas important for energy homeostasis regulation, including the arcuate nucleus (Arc), lateral hypothalamic area (LHA), paraventricular nucleus (PVN), and dorsomedial hypothalamic nucleus [10,11]. However, studies of CART primarily conducted in rodents have so far generated inconclusive or discrepant results [1], highlighting the complexity in the physiology of endogenous CART biosynthesis and function. In rats and mice, in addition to alternative splicing of Cart mRNA on the transcription level, the resultant CART propeptides harbor several cleavage sites that are subjected to post-translational processing by prohormone convertases, which exhibit tissue- and brain region-specific expressions and functions [8,11,12]. Hence, the in vivo production of several CART isoforms also involves processing and expression in a tissue- and site-specific manner [8,12], generating at least two predicted active CART peptides, CART I (42-89/55-102) and CART II (49-89/62-102) [5,13]. Accordingly, studies in rodents have suggested the differential physiological functions of CART variants across the periphery as well as the central nervous system [8].

In light of the multiple factors involving complex region-specific post-translational processing, along with undetermined conformational profile and binding sites for the peptide, studies are challenged with limited targeting contacts to mimic or modulate endogenous CART expression and activity. Although most traditional studies have classified CART as anorexigenic [14—16], orexigenic evidences also exist [17—19]. In mouse models, global CART knockout led to an overall increase in body weight gain and adiposity, while lacking any overt impact on food consumption [1,20]. Supporting the catabolic property of CART, mutations and polymorphisms in the human CART gene are linked to obesity and associated metabolic disorders [21,22]. On the other hand, while intracerebroventricular (i.c.v.) administration of various CART isoforms in rodents consistently and dose-dependently suppressed food intake and weight gain [1,23], overexpression of CART I (55-102) in specific hypothalamic nuclei was shown to induce either stimulatory or inhibitory response on feeding and body weight [17,18,24]. This suggests that CART originating from different nuclei is engaged in differential functions involving discrete neurocircuitries. Furthermore, central administrations of different CART variants, which demonstrate varying endogenous abundance in distinct brain regions, have exhibited site-specific activities and differential potencies in affecting food intake and body weight gain [25,26].

In an effort to identify the most critical hypothalamic sites of CART action in the control of energy homeostasis, the Arc and LHA have received considerable interest. The Arc represents a pivotal structure for adiposity signal integration and metabolic modulation [27], where CART expression is enriched and colocalized with the anorexigenic proopiomelanocortin (POMC) [28,29]. The first-order CART-containing neurons at the Arc launch axonal projections to neurons at the LHA and PVN [30—32]. Despite implications for the Arc-LHA pathway in mediating the anorexic effects of CART [30,31], direct injection of CART into the Arc or LHA in rodents triggered overt orexigenic responses [17,18,24]. Differential neurochemical responses were also shown at the two regions. For instance, while Cart mRNA levels at the Arc are markedly reduced by fasting and restored following refeeding [33,34], such correlation was not demonstrated at the LHA [35]. Moreover, CART in the LHA is found to be colocalized with the orexigenic-acting melanin-concentrating hormone (MCH) [36,37], further hinting that CART in different hypothalamic areas and neurons may exhibit disparate functions.

In this study, we aimed to more specifically investigate the effects of CART in the Arc and LHA on the regulation of feeding and energy homeostasis. For this, we developed models that allow the CART neuron-specific introduction and processing of CART by combining Cart-cre knock-in mice with a Cart adeno-associated viral vector designed using the flip-excision switch (AAV-FLEX) technology [38]. The AAV vector encodes the long form of the mouse Cart cDNA CART I (55-102), which is focused herein due to wider documentation and the reported higher potency in influencing appetite and body weight compared to the CART II (62-102) isoform [25,39]. This approach allows for either reintroducing CART specifically into CART neurons in otherwise CART-deficient mice, or to overproducing CART in Arc or LHA CART neurons, avoiding off-target side-effects associated with simple ectopic delivery. Furthermore, our viral approach also facilitates the in vivo processing and modifications of CART propeptides in a natural physiological environment, hence producing active peptides under endogenous conditions. Mouse models generated this way were then analyzed in a comprehensive phenotyping paradigm, determining all major aspects that are involved in energy homeostasis control.

2. MATERIALS AND METHODS

2.1. Animals
All research and animal care procedures were approved by the Garvan Institute/St. Vincent's Hospital Animal Ethics Committee and were conducted in agreement with the Australian Code of Practice for the Care and Use of Animals for Scientific Purposes. Male mice were used for all experiments and were housed under conditions of controlled temperature (22 °C) and illumination (12:12 h light—dark cycle, lights on at 07:00 am). Mice were provided with ad libitum access to water and standard chow diet (8% calories from fat, 21% calories from protein, 71% calories from carbohydrate, 2.6 kcal/g; Gordon's Specialty Stock Feeds, Yanderra, NSW, Australia).

2.2. Generation of inducible Cart-cre knock-in mouse model
To investigate the effects of CART action at particular hypothalamic regions, CART neuron-specific introduction of genetic elements was performed in an adult-onset inducible manner. This is enabled through the use of a conditional Cart-cre knock-in mouse line, for which the detailed generating procedures were described previously [20]. As illustrated [20], the inducible Cart-cre knock-in mice (Cart^{cre/cre}) were generated by crossing the Cart^{lox/lox} line with mice that expressed Cre-recombinase specifically in the oocytes to homozygosity, hence combining the tamoxifen-inducible Cre gene with the endogenous Cart promoter. In this study, both the homozygous Cart^{cre/cre} and the heterozygous Cart^{cre/+} mouse lines were included. Comparison between the two groups serves to highlight the contribution of CART function in specific hypothalamic nuclei to feeding and metabolic regulation in the presence or absence of endogenous CART signaling.

2.3. Generation and expression of cre-inducible AAV-FLEX-Cart vector
To selectively express the bioactive CART in CART neurons, the flip-excision switch technique was employed to create a unique Cre-recombinase-dependent AAV vector for delivery, which carries a double floxed inverted open reading frame (Figure 1). The FLEX strategy utilizes the recombination mechanism whereby DNA elements flanked by loxP recombination sites in the opposite orientation are inverted by Cre-recombinase [38]. The AAV-FLEX-Cart vector consists of a codon-optimized mouse Cart cDNA for the expression of CART I (55-102) active peptide flanked by loxP-sites as displayed in Figure 1A.

Original Article

Gene expression is driven by the chicken β-actin (CBA) promoter on a self-complementary AAV vector backbone packaged in AAV capsids of serotype 1. AAV vectors are produced by plasmid cotransfection of HEK293 cells, benzonase-treatment of cell extracts and purification by high-performance liquid chromatography using AVB-Sepharose columns, as described [40].

Within this *AAV-FLEX-Cart* vector, the *Cart* coding sequence is flanked by a set of two distinct *loxP* sites positioned in the opposite orientation to each other (Figure 1Ai), where recombination only occurs between the same type of *loxP* sequences. The *Cart* coding unit was placed in a reverse thus inactive orientation downstream of the CBA promoter, preventing expression prior to Cre-driven recombination. Upon exposure to tamoxifen, Cre-recombinase is activated through translocation from the cytoplasm to the nucleus, thereby catalyzing the inversion of the *loxP*-flanked cassette in two possible ways (Figure 1Aii). Subsequent recombination between the same type of *loxP* sites placed in the same orientation would eliminate the alternative *loxP* site in-between, thereby generating the stable transgene with the *Cart* sequence in the correct orientation for further transcription and translation (Figure 1Aiii). In parallel, *AAV-FLEX-GFP* encoding the green fluorescence protein (GFP) was used as the control. As Cre expression is driven by the endogenous *Cart* promoter in the *Cart-cre* knock-in mice, the *AAV-FLEX-Cart* vector and the *AAV-FLEX-GFP* control are targeted only to CART neurons. Hence, production of the active form of CART or GFP is exclusive to CART neurons.

2.4. Stereotaxic delivery of *AAV-FLEX-Cart* to CART neurons in *Cart-cre* knock-in mice

Adult-onset central CART neuron-specific expression of CART I (55-102) in the Arc or LHA was achieved by intra-hypothalamic injection of the *AAV-FLEX-Cart* vector in parallel with i.c.v. tamoxifen administration in *Cart-cre* knock-in mice. At 11 weeks of age, $Cart^{cre/cre}$ and $Cart^{cre/+}$ mice were anesthetized with intraperitoneal (i.p.) injection of 100/20 mg/kg ketamine/xylazine (Parke Davis-Pfizer, Sydney, Australia & Bayer AG, Leverkusen, Germany) and immobilized in a stereotaxic frame (David Kopf Instruments, Tulunga, CA, USA) in the flat-skull position. A small incision was made to expose the skull, where a small hole was opened for injection. One microliter of the *AAV-FLEX-Cart* vector (titer 1.0×10^{12} viral particles/ml) or the *AAV-FLEX-GFP* control vector was injected unilaterally into the Arc or LHA at a speed of 0.1 μl/min using a 2-μL Hamilton syringe connected to a syringe infusion pump (World Precision Instruments Inc., Waltham, MA, USA). The *AAV-FLEX-Cart* or *AAV-FLEX-GFP* was stereotaxically delivered into both $Cart^{cre/cre}$ and $Cart^{cre/+}$ mice, such that mice from each genotype were separated into two groups, one injected at the right Arc (coordinates relative to Bregma: -2.18 mm anteroposterior, -0.25 mm mediolateral, and -5.5 mm dorsoventral), and the other injected at the right LHA (coordinates relative to Bregma: -1.94 mm anteroposterior, -1.0 mm mediolateral, and -5.25 mm dorsoventral). Mice from each of the four groups were further divided evenly into two groups based on body weight and fat mass, one receiving the *AAV-FLEX-Cart* injection and the other littermate group injected with the *AAV-FLEX-GFP* control. The injection needle was gently withdrawn 15 min after injection. To activate the *Cre*-recombinase for mediating the transgene inversion and expression, 1 μl of the active metabolite of tamoxifen 4-OHT [41] (20 mg/mL) (Sigma–Aldrich Pty Ltd, Sydney, NSW, Australia) dissolved in absolute ethanol was then injected unilaterally into the left lateral cerebral ventricle (LV) at a rate of 0.1 μl/min using a 2-μl Hamilton syringe (World Precision Instruments Inc.). The injection coordinates relative to

Bregma were -0.34 mm anteroposterior, $+1.0$ mm mediolateral, and -2.5 mm dorsoventral corresponding to the left LV [42]. Body temperature of the animals was maintained by placement on a heating pad throughout the surgical process and the overnight recovery period. Mice were allowed two weeks of recovery with regular body weight assessment prior to any phenotypic characterization procedures. According to previous experience from extensive central viral delivery experiments [43], maximal expression of the transgene is estimated to be reached within two weeks and remain stable for at least 6 months. The conditional tamoxifen-induced Cre activation and concomitant intranuclear delivery of *AAV-FLEX-Cart* or *AAV-FLEX-GFP* in the hypothalamus resulted in $Cart^{cre/cre}$ and $Cart^{cre/+}$ mice with CART or GFP selectively expressed in CART neurons at the Arc or LHA. For simplicity, the post-surgery subjects are referred to as Arc^{CART} or Arc^{GFP};$Cart^{cre/cre}$ or $Cart^{cre/+}$, and LHA^{CART} or LHA^{GFP};$Cart^{cre/cre}$ or $Cart^{cre/+}$ mice. At least 10 mice were included for each of the resultant 8 groups, with $n = 10-12$ for each site of injection with either CART or GFP for each genotype. For each targeted area and each genotype, at least two cohorts of animals were used, each cohort consisting of *AAV-FLEX-Cart*-injected mice run in parallel with *AAV-FLEX-GFP*-injected mice from the same litter.

2.5. Verification of the expression site of targeted *AAV-FLEX-Cart* by *in situ* hybridization and immunohistochemistry

To validate the injection sites at the hypothalamic Arc or LHA regions where CART was introduced to CART neurons, and to verify functionality of the *AAV-FLEX-Cart* construct, *in situ* hybridization and immunostaining for CART mRNA and protein expression were examined in brains collected from *Cart-cre* knock-in mice. At the transcriptional level, efficiency of *Cart* reintroduction or overexpression was validated by *in situ* hybridization for *Cart* mRNA on brain cryosections from both the Arc$^{CART/GFP}$ and LHA$^{CART/GFP}$ $Cart^{cre/cre}$ and $Cart^{cre/+}$ mice ($n = 5$ each) following procedures as described above.

For the detection of CART-containing cells receiving *AAV-FLEX-Cart* delivery at the translational level, CART peptide expression was assessed by immunohistochemistry as previously described [20,43]. At the completion of study, a separate group of mice was anesthetized with i.p. injection of 100/20 mg/kg ketamine/xylazine (Parke Davis-Pfizer) and sacrificed via transcardial perfusion. The brains were subsequently fixed by perfusion and subjected to post-fixing and cryoprotection. Coronal brain slices (30 μm) from both the Arc^{CART} and LHA^{CART} $Cart^{cre/cre}$ and $Cart^{cre/+}$ mice ($n \geq 5$ each) were serially cryosectioned and incubated overnight with rabbit anti-mouse CART polyclonal primary antibody Ca7-OVA [44] (gift from Dr. Anna Secher, Novo Nordisk, Copenhagen, Denmark) diluted 1:1500. Sections were then incubated with biotinylated goat anti-rabbit IgG secondary antibody (Vector Laboratories, Burlingame, CA, USA) diluted 1:250 for 2 h, followed by incubation with ExtrAvidin-peroxidase (Sigma–Aldrich, St. Louis, MO, USA). Immunostaining for CART expression was performed using diaminobenzidine (Dako, Carpinteria, CA, USA) as the chromogen. Free-floating brain sections were mounted on Superfrost® glass slides (Menzel-Glaser, Braunschweig, Germany) and coverslipped. For visualization of CART immunoreactivity (IR), brain sections containing the targeted Arc or LHA regions from respective mice were investigated using a Zeiss Axiophot microscope equipped with a ProgRes 3008 digital camera (Carl Zeiss, Jena, Germany). Bright field photomicrographs were acquired for the targeted hypothalamic regions on both the injection and contralateral sides of the brain for comparison. An increase in CART-IR on the injection side relative to the contralateral side therefore signifies the presence of AAV-delivered
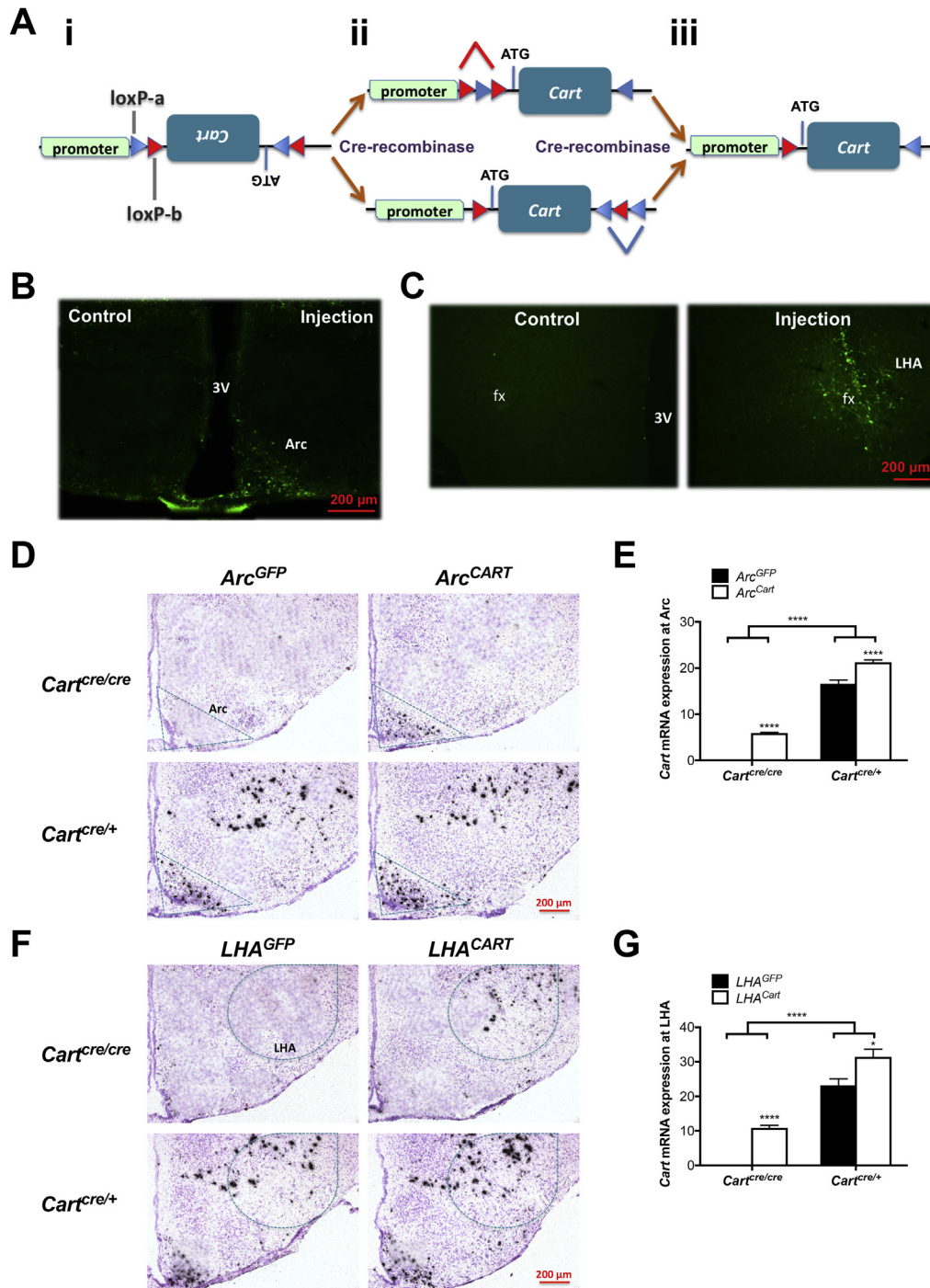
Figure 1: (A) Schematic representation of the *AAV-FLEX-Cart* vector targeted selectively to CART neurons in the Arc or LHA in *Cart-cre* knock-in mice. The Cre-inducible *Cart* AAV vector was designed using the FLEX switch strategy. (**i**) The targeting construct comprises the CBA promoter, followed by two pairs of heterotypic recombinase recognition *loxP* sites (here referred to as *loxP-a* and *loxP-b*) in antiparallel configuration, flanking the codon-optimized *Cart* coding region in the anti-sense inactive orientation relative to the promoter. (**ii**) Administration of tamoxifen activates Cre expression driven by the endogenous *Cart* promoter to mediate inversion of the floxed element in two possible manners, whereby subsequent recombination occurs among the same type of *loxP* sites. Consequently, parallel *loxP* sites of the same type recombine, namely *loxP-a* with *loxP-a*, *loxP-b* with *loxP-b*, deleting the alternative *loxP* type in-between. (**iii**) Stable transgene consisting of the *Cart* coding unit in an orientation parallel to the promoter is transcribed and translated into bioactive and functional CART peptide, which is expressed specifically in the targeted CART neurons in the hypothalamus. Figure 1B—C: Representative fluorescence micrographs of coronal brain sections from *Cart$^{cre/cre}$* and *Cart$^{cre/+}$* mice unilaterally injected with the *AAV-FLEX-GFP* control, displaying the Arc (**B**) and LHA (**C**) regions where GFP expression within the targeted neurons indicates accurate stereotaxic delivery. Figure 1D—G: Confirmation of *Cart* reintroduction and overexpression in the Arc and LHA by *in situ* hybridization in *Cart-cre* knock-in mice. Representative bright-field photomicrographs of coronal brain sections showing *Cart* mRNA at the Arc (**D**) and LHA (**F**) of *Cart$^{cre/cre}$* and *Cart$^{cre/+}$* mice receiving *AAV-FLEX-Cart* versus *AAV-FLEX-GFP* injection. Scale bar = 200 μm. Hybridization signals at the Arc (**E**) and LHA (**G**) of respective brain sections are quantified as mean labeling intensity of neurons expressed as percentage coverage of neuronal surface by silver grains (RODs) within the defined areas of interest. 3V, third ventricle; fx, fornix; Arc, arcuate nucleus; LHA, lateral hypothalamic area. Data are means ± SEM and averaged for all mice from each group examined. ****$p \leq 0.0001$ for *Cart$^{cre/cre}$* or *Cart$^{cre/+}$* mice targeted with *AAV-Cart* versus *AAV-GFP* in the Arc or LHA, or for comparisons between different genotypes receiving the same treatments.

CART-expressing CART neurons that are accurately targeted and functional.

In parallel, brain sections from a portion of the $Cart^{cre/cre}$ and $Cart^{cre/+}$ mice with *AAV-FLEX-GFP* targeted into the Arc or LHA (n = 3 each) were prepared as described above and mounted on Superfrost® slides for the detection of GFP expression by direct fluorescence microscopy. To detect GFP expression produced by the control targeting construct, brain sections containing the targeted Arc or LHA regions from respective mice were examined using a Leica DM5500 B fluorescent microscope (Leica, Chicago, IL, USA). Fluorescence micrographs were acquired for the visualization of GFP, indicative of successful delivery and expression of the empty control vector in CART neurons at the respective areas.

2.6. Determination of food intake and body weight

All $Cart^{cre/cre}$ and $Cart^{cre/+}$ mice were fed a standard laboratory chow and subjected to the same experimental procedures as follows. Body weight was measured weekly throughout the duration of studies. Following a two-week recovery period after the brain surgery, all mice were at 13—14 weeks of age. Mice were assessed for spontaneous food intake in the fed state as well as for fasting-induced food intake in response to 24-hr fasting. Basal daily food intake was determined as the average of duplicate readings obtained over two consecutive 24-hr periods. Twenty four-hr fasting-induced food intake was subsequently measured at 1, 3, 7, and 24 h after refeeding, while the corresponding body weight was recorded in parallel.

2.7. Indirect calorimetry of energy expenditure and assessment of physical activity

All $Cart^{cre/cre}$ and $Cart^{cre/+}$ mice with Arc^{CART} or LHA^{CART} together with the controls Arc^{GFP} or LHA^{GFP} (n = 10 - 12 per group) were evaluated for metabolic parameters and physical activity at 16—17 weeks of age. For energy metabolism, metabolic rate was measured by indirect calorimetry using an 8-chamber open-circuit calorimeter (Oxymax series; Columbus Instruments, Columbus, OH, USA). For each 24-hr run, 4 mice targeted with *AAV-Cart* in a specific region were matched with 4 control mice of the same genotype with *AAV-GFP* in the same region. Hence, with n = 10—12 per group, three runs were involved for *AAV-Cart* mice in parallel with *AAV-GFP* mice for each targeted area for each genotype. Mice were housed individually in specially built Plexiglas cages with airflow of 0.6 L/min at a consistent ambient temperature of 22 °C, following standard protocol as previously described [45]. Oxygen consumption (VO$_2$) and carbon dioxide production (VCO$_2$) were measured every 27-min intervals. The respiratory exchange ratio (RER) was calculated as the quotient of VCO$_2$/VO$_2$, with 100% carbohydrate oxidation represented by the value of 1.0 and 100% fat oxidation the value of 0.7. Energy expenditure (kcal heat produced) was determined as calorific value (CV) $\times$ VO$_2$, where CV is 3.815 + 1.232 $\times$ RER. Data obtained for the 24-hr monitoring period were averaged at 1-hr intervals for energy expenditure and RER.

For physical activity, ambulatory activity of the mice was assessed in parallel within the Plexiglas metabolic chambers with an OPTO-M3 sensor system (Columbus Instruments). Ambulatory counts denote the consecutive adjacent photo-beam breaks, while cumulative ambulatory counts of the X, Y and Z directions were recorded per minute and summed at 1-hr intervals.

2.8. Body composition and bone densitometry analysis

All mice from both $Cart^{cre/cre}$ and $Cart^{cre/+}$ groups were subjected to body composition analysis using the dual-energy X-ray absorptiometry (DXA, Lunar PIXImus2 mouse densitometer; GE Healthcare, Waukesha, WI, USA) system at 16—17 weeks of age, immediately following completion of the indirect calorimetry assessment of energy metabolism and physical activity. Animals were anesthetized with isoflurane for the scanning procedure to determine whole body bone mineral density (BMD), bone mineral content (BMC), fat and lean mass, where lean mass corresponds to non-fat and non-bone tissue content. The head of the animal was excluded while the tail included for the analysis.

2.9. Measurement of whole body and brown adipose tissue temperatures by infrared imaging

Whole body temperature and temperature of the interscapular brown adipose tissue (IBAT) were measured for both the $Cart^{cre/cre}$ and $Cart^{cre/+}$ cohorts by non-invasive high-sensitivity infrared imaging as described previously [20]. Briefly, all 17-week-old mice were transferred from group housing to individual cages for acclimatization 2 days prior to imaging procedures. For area-specific exposure of skin to facilitate temperature reading, all mice were shaved at the IBAT and lumbar back regions under light isoflurane anesthesia in parallel. A high-sensitivity infrared camera (ThermoCAM T640, FLIR, Danderyd, Sweden, sensitivity = 0.04 °C) fixed on a tripod was placed 100 cm above the freely moving singly housed mouse, and thermographic images were taken for 1 min per mouse. After each 1-min measurement, the camera was moved to record surface temperatures of the next mouse. Temperature measurement was performed daily for three consecutive days.

2.10. Glucose metabolism studies

All mice from both $Cart^{cre/cre}$ and $Cart^{cre/+}$ cohorts were examined by intraperitoneal glucose tolerance test (IPGTT) and insulin tolerance test (IPITT). IPGTT and IPITT were conducted at 15 and 18 weeks of age, respectively. For IPGTT, mice were subjected to 6-hr fasting; food was removed from cage hoppers at 09:00 h and injection of a dose of a 10% D-glucose solution (1.0 g/kg body weight; Astra Zeneca, North Ryde, NSW, Australia) was performed 6 h later into the peritoneal cavity. For IPITT, mice were subjected to 5-hr fasting where food was removed from cage hoppers at 10:00 h and injection of a dose of insulin (0.5 IU/kg body weight) (Novo Nordisk Pharmaceuticals, Baulkham Hills, NSW, Australia) was performed 5 h later into the peritoneal cavity. For both tests, tail vein blood was collected at 0, 15, 30, 60, and 90 min following glucose or insulin injection, and glucose concentrations were measured using a glucometer (Accu-Check II; Roche, Castle Hill, NSW, Australia). For IPGTT, insulin levels were subsequently quantified using a sensitive rat insulin radioimmunoassay (RIA) kit (Millipore, Billerica, MA, USA). Glucose and insulin tolerance curves constructed for the glucose levels obtained during IPGTT and IPITT respectively are presented in terms of absolute values. Area under the glucose (AUCglucose) or insulin (AUCinsulin) concentration curves between 0 and 90 min after glucose injection during IPGTT were plotted after subtraction of the initial concentrations prior to injection.

2.11. Tissue collection

Following completion of studies, all mice from both $Cart^{cre/cre}$ and $Cart^{cre/+}$ groups were sacrificed at 19 weeks of age. Animals were culled between 13:00 to 17:00 h through cervical dislocation followed by decapitation. Brains were promptly collected and frozen on dry ice, then stored at −80 °C until subsequent analysis as described below. The brown adipose tissue (BAT) at the interscapular area and the white adipose tissue (WAT) depots from the inguinal, epididymal,

retroperitoneal and mesenteric regions were removed and weighed. Major organs including the pancreas, liver, gonads, heart, kidney, seminal vesicles, and spleen were also removed and weighed.

2.12. *In situ* hybridization analysis of key hypothalamic neuropeptides

In situ hybridization was performed on brain sections of $Cart^{cre/cre}$ and $Cart^{cre/+}$ mice from both the Arc$^{CART/GFP}$ and LHA$^{CART/GFP}$ groups (n = 5 each) to determine mRNA expression of *Cart*, *Pomc*, neuropeptide Y (*Npy*), corticotropin-releasing hormone (*Crh*), *Mch*, orexin (*Orx*), tyrosine hydroxylase (*Th*), and thyrotropin-releasing hormone (*Trh*) at the hypothalamus following procedures as previously described [20]. Briefly, matching coronal brain sections (25 μm) collected from the *Cart-cre* knock-in mice were prepared from specific brain levels with respect to the Bregma to represent the hypothalamic areas involved in the regulation of energy homeostasis. Detection of the mRNA expression was performed for *Cart* in the Arc and LHA, for *Npy* and *Pomc* in the Arc, for *Mch* and *Orx* in the LHA, and for *Crh, Th,* and *Trh* in the PVN. The cryosections were hybridized with [α-^{35}S]-thio-dATP (PerkinElmer, Boston, MA, USA) radiolabeled DNA oligonucleotides complementary to mouse *Cart:* (5′-TCCTTCTCGTGGGACGCATCATC-CACGGCAGAGTAGATGTCC AGG-3′), *Pomc:* (5′-TGGCTGCTCTCCAGG-CACCAGCTCCACACATCTATG GAGG-3′), *Npy:* (5′-GAGGGTCAGTCCACA CAGCCCCATTCGCTTG TTACCTA GCAT-3′), *Crh:* (5′-CCGATAATCTC CATCAGTTTCCTGTTGCTGTGAGC TTGCTGAGCT-3′), *Mch:* (5′-TTTCCTG TGTGGACTCAGCATTCTGAACTCCAT TCTCAGCTGG-3′), *Orx:* (5′-CTTTCCCAGAGTCAGGATACCCGCAGCGTGGT TGCCAGCTCCGTGC-3′), *Th:* (5′-CTCTAAGGAGCGCCGGATGGTGTGAGGA CTGTCCAGTACATCA-3′) and *Trh:* (5′-AACCTTACTCCTCCAGAGGTTCCCT GACCCAGGCTTC-CAGTTGTG-3′). Hybridization signals on sections were visualized by exposure to BioMax MR film (Kodak, Rochester, NY, USA) for 7—10 days and digitalized images from the scanned autoradiograms were acquired. For structural details, the brain sections were photoemulsion-dipped and superficially counterstained with hematoxylin, with which regions of interest were visualized and captured into digital images acquired by bright-field microscopy. Quantification of the mRNA expression levels of respective genes was performed by measuring the relative optical densities (RODs) within the brain areas of interest outlined with consistent defined dimensions across corresponding sections on the photomicrographs using the National Institutes of Health ImageJ 1.61 software (written by Wayne Rasband; available at https://imagej.nih.gov/ij/). Background labeling was considered uniform with signal levels below 5% of specific signal levels and was subtracted from the resultant signal density. Data are evaluated and presented as percentage of ROD averaged from at least three sections per mRNA assessed per animal.

2.13. Statistical analysis

All data are presented as means ± SEM. Differences among mouse groups of various genotypes and viral treatments were assessed by ANOVA or repeated-measures ANOVA combined with Bonferroni post-hoc analysis where appropriate. Energy expenditure, RER, and physical activity over the continuous 24-hr period were averaged for the whole 24-hr period, as well as the 12-hr light and dark phases individually. Comparison of energy expenditure (kcal/hr) between groups was performed by the analysis of covariance (ANCOVA) with lean mass as the covariate. The adjusted means of energy expenditure at a common lean mass for the comparison were generated by ANCOVA as presented. Statistical analyses were performed with GraphPad Prism 7 for Mac OS X (GraphPad Software, Inc. CA, USA). Statistical significance was defined as p-value ≤ 0.05.

3. RESULTS

3.1. Generation of hypothalamic CART neuron-specific re-introducing or overexpressing CART mouse models

To investigate the role of CART in the Arc and LHA, we employed our inducible *Cart-cre* knock-in lines selectively injected with AAV1-FLEX-CART vectors into these two brain areas. Specifically we used heterozygous $Cart^{cre/+}$ mice, which allow for the CART neuron-specific overexpression of CART, as well as homozygous $Cart^{cre/cre}$ mice with global CART ablation, thus allowing for the CART neuron-specific reintroduction of CART on an otherwise CART-deficient background [20].

To demonstrate the precise delivery of the construct to the targeted brain regions, we first employed the GFP reporter for visual guidance. Two weeks after *AAV-FLEX-GFP* injection, GFP expression was detected exclusively in either the Arc (Figs. 1B and S1A) or LHA (Figs. 1C and S1B), as shown in the representative photomicrographs, validating accurate targeting of the viral vectors. Next, to verify targeted expression and functionality of the unilaterally injected *AAV-FLEX-Cart* construct, which was activated through i.c.v. tamoxifen treatment, CART neuron-specific introduction of CART expression was determined on both the transcriptional and translational levels. Successful *Cart* reintroduction was confirmed by *in situ* hybridization in both the Arc (Figure 1D—E) and LHA (Figure 1F—G) of $Cart^{cre/cre}$ mice, where *Cart* mRNA expression was only observed in mice receiving *AAV-FLEX-Cart* while absent in control groups treated with *AAV-FLEX-GFP*. In parallel, $Cart^{cre/+}$ mice subjected to Arc (Figure 1D—E) or LHA (Figure 1F—G) CART AAV overexpression displayed significantly upregulated *Cart* mRNA expression in the corresponding areas compared to the respective *AAV-FLEX-GFP* controls of the same genotype.

Immunostaining for CART protein expression further confirmed the exclusive CART-IR shown on the injection side, but not on the contralateral control side, for both the Arc (Figure 2A) and LHA (Figure 2B) regions in $Cart^{cre/cre}$ mice receiving *AAV-Cart* unilaterally. CART immunostaining at the respective local sites of delivery (Figure 2A—B) displayed a pattern that is consistent with endogenous CART-containing neurons [2,3], signifying selective CART reintroduction in CART neurons only. In contrast, lack of CART-IR on the contralateral sides (Figure 2A—B) denotes the regional and CART neuron-specific targeting, with minimal diffusion to other areas in the brain. No CART-IR was detected on matching sections from Arc^{GFP} or LHA^{GFP};$Cart^{cre/cre}$ controls (Figure 2A—B). Similarly, notably higher CART-IR was shown on the injection compared to the contralateral side for both the Arc (Figure 2A) and LHA (Figure 2B) in $Cart^{cre/+}$ mice treated with *AAV-CART*. Such difference was not observed in $Cart^{cre/+}$ counterparts receiving Arc^{GFP} (Figure 2A) or LHA^{GFP} control constructs (Figure 2B). The visual guidance from CART expression further verified the correct stereotaxic injection for both Arc and LHA groups, while only data from mice identified for positive hits were used for downstream analysis.

3.2. Selective reintroduction of CART in CART neurons in the arc but not the LHA reduces body weight

To investigate the basic metabolic characteristics of $Cart^{cre/cre}$ and $Cart^{cre/+}$ mice re-introduced with or overexpressing CART in the (Arc^{CART}) or (LHA^{CART}), male mice at the age of 11 weeks were unilaterally injected with *AAV-FLEX-Cart* or *AAV-FLEX-GFP* into the Arc or LHA, respectively, and body weight and other metabolic parameters were measured following the targeted brain surgery.

In $Cart^{cre/+}$ mice with endogenous CART expression in place, CART overexpression targeted at either the Arc (Figure 3A) or LHA (Figure 3B) had no obvious effect on body weight compared with respective
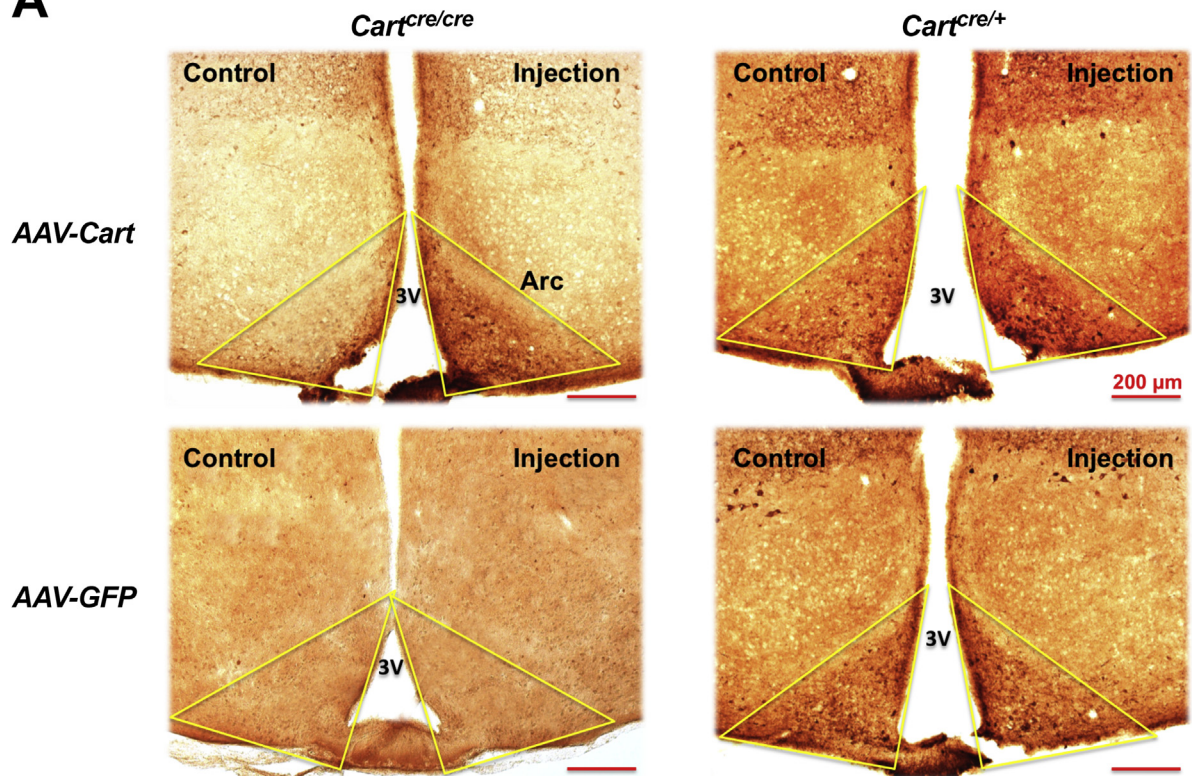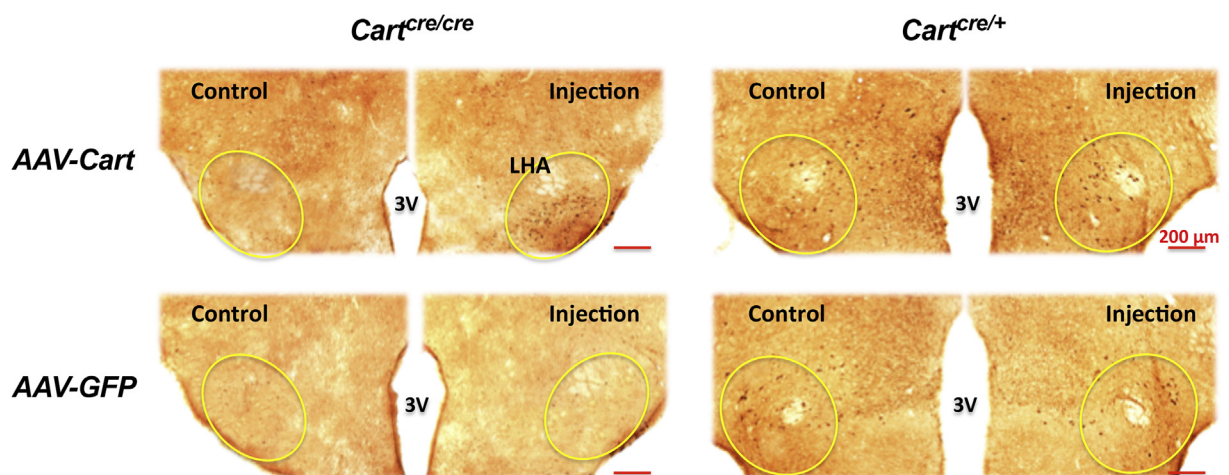
Figure 2: Validation of the site-specific reintroduction and overexpression of CART peptide in *Cart-cre* knock-in mice by immunohistochemistry. Representative bright-field photomicrographs of CART-immunostained matching brain sections from *Cart$^{cre/cre}$* and *Cart$^{cre/+}$* mice unilaterally injected with the *AAV-FLEX*-GFP control or AAV-*FLEX-Cart* in the Arc (**A**) or LHA (**B**). Left panel: high densities of CART immunostaining within CART neurons at the Arc or LHA were only shown on the injection side of the respective brain sections from *Cart$^{cre/cre}$* mice receiving *AAV-Cart* but not *AAV-GFP*. CART-IR exhibited a pattern concordant with endogenous CART-containing neurons, while lacking on the contralateral control side. Right panel: higher CART-IR was shown in the Arc or LHA on the injection compared to the contralateral side of brain sections from *Cart$^{cre/+}$* mice targeted with *AAV-Cart*, whereas comparable CART-IR was displayed on both sides for counterparts treated with *AAV-GFP*. Scale bar = 200 μm. 3V, third ventricle; fx, fornix; Arc, arcuate nucleus; LHA, lateral hypothalamic are.

controls injected with the *AAV-GFP* control construct. The lack of difference was seen for both absolute body weight as well as weight gain expressed as a percentage of initial body weight (Figure 3A—B). In contrast, in *Cart$^{cre/cre}$* mice without endogenous CART expression, CART reintroduction into the Arc CART neurons led to a significant

decrease in both absolute body weight and percentage weight gain compared to *AAV-GFP* controls over the entire study period (Figure 3C). On the contrary, no significant effect on body weight was seen after CART was reintroduced into the LHA of *Cart$^{cre/cre}$* mice (Figure 3D). These results suggest that CART action originating from the Arc but not
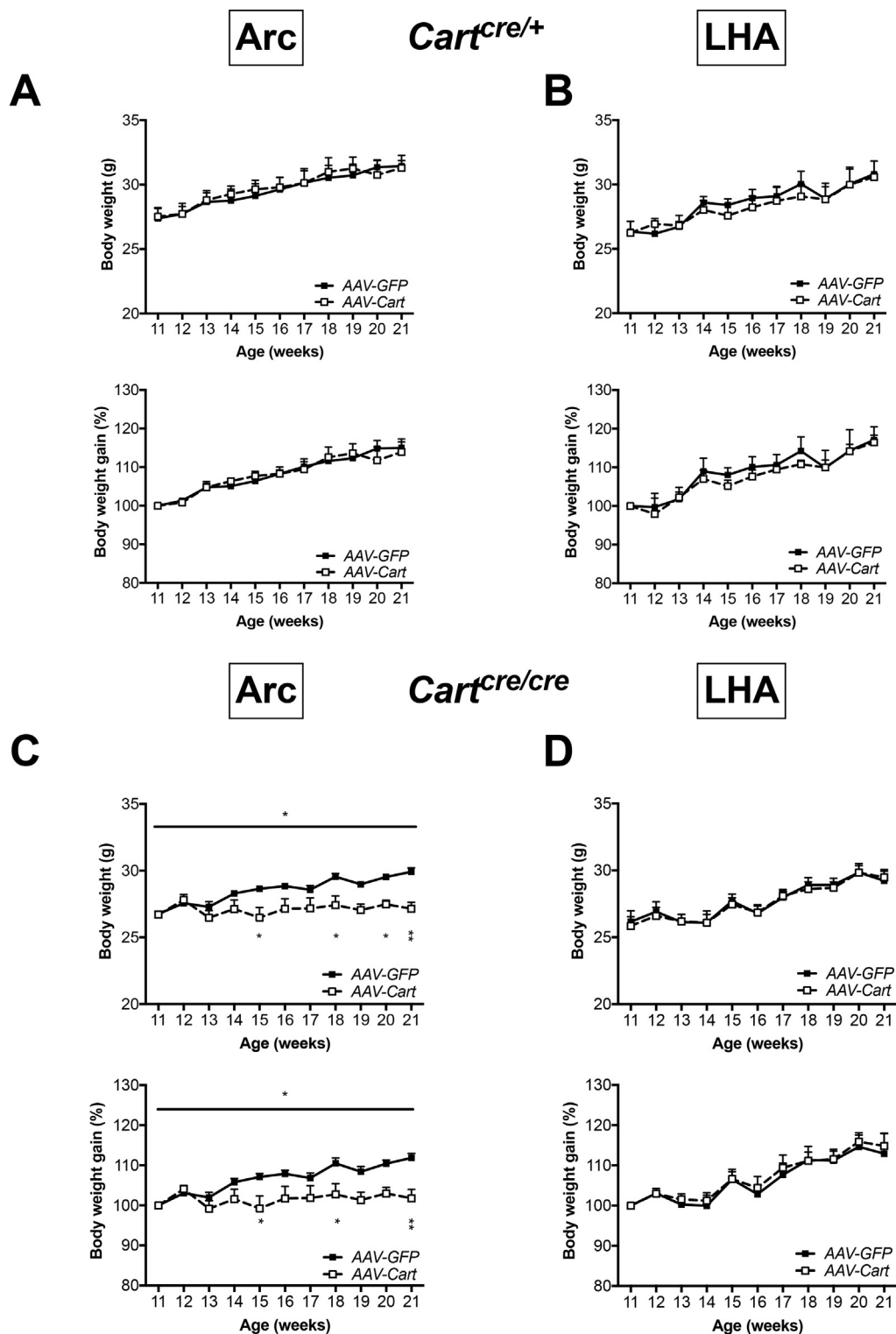
Figure 3: Specific introduction of CART expression into CART neurons in the Arc led to significant decline in body weight in homozygous $Cart^{cre/cre}$ but not heterozygous $Cart^{cre/+}$ mice. Absolute body weight and corresponding body weight change as a percentage of initial body weight measured weekly in $Cart^{cre/+}$ (**A - B**) and $Cart^{cre/cre}$ (**C - D**) mice targeted with *AAV-Cart* or *AAV-GFP* in the Arc (**A, C**) or the LHA (**B, D**) (n = 10 - 12 per group). Data are means ± SEM and averaged for all mice from each group examined. *$p \leq 0.05$, **$p \leq 0.01$ for *AAV-Cart* versus *AAV-GFP* treatments, or for comparisons indicated by horizontal bar.

the LHA is responsible for the establishment of a negative energy balance that is leading to a body weight loss.

3.3. CART neuron-specific rescue of CART expression in the arc and LHA leads to opposite effects on adiposity

To elucidate the factors contributing to the differential responses in body weight to CART delivery, body composition analysis was performed. In line with the markedly lower body weight (Figure 3C), $Cart^{cre/cre}$ mice expressing Arc^{CART} demonstrated a significant decrease in whole body fat mass compared with Arc^{GFP} controls (Figure 4A), as confirmed by the significantly reduced mass of

dissected white adipose tissue depots (Figure 4B). Interestingly, whole body lean mass was unaltered following Arc CART reintroduction (Figure 4C). In contrast, despite similar body weight, $Cart^{cre/cre}$ mice with CART rescue in the LHA exhibited a significant increase in whole body fat mass (Figure 4D) compared to the $AAV\text{-}GFP$ controls, consistent with the markedly higher dissected fat weights (Figure 4E). Unlike the Arc CART reintroduction, rescue of CART in the LHA was accompanied by a significant reduction in lean mass relative to LHA^{GFP} counterparts (Figure 4F). The lower lean mass may have offset the greater fat mass (Figure 4D–E), leading to the unvaried absolute body weight observed (Figure 3D). It is therefore possible, while not directly
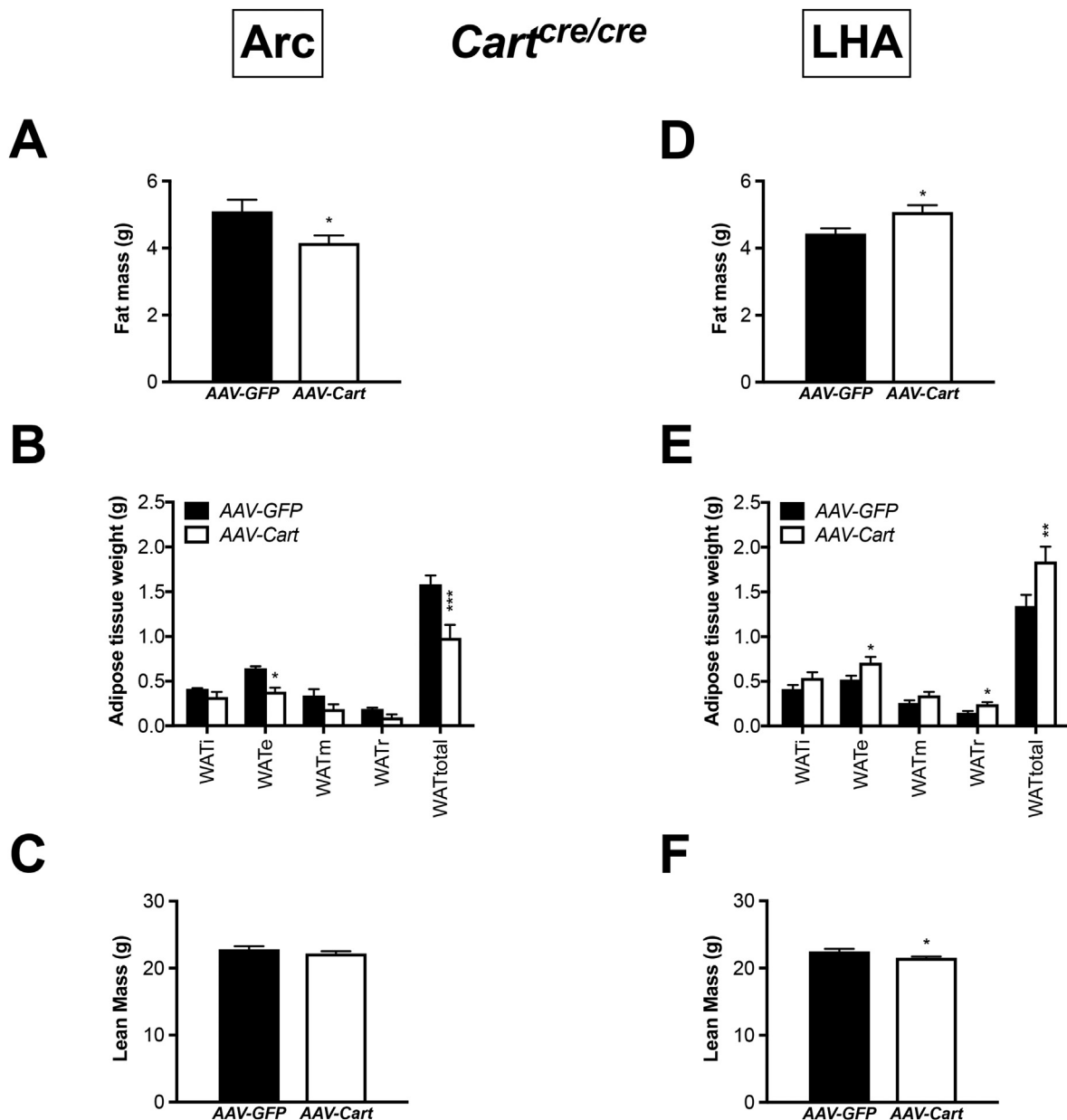
Figure 4: Reintroduced CART expression in CART neurons in the Arc and LHA reduces and increases fat mass respectively in $Cart^{cre/cre}$ mice. Body composition analysis using dual-energy X-ray absorptiometry. Whole body fat mass in $Cart^{cre/cre}$ mice injected with Arc^{CART} versus Arc^{GFP} (**A**) or LHA^{CART} versus LHA^{GFP} (**D**) (n = 10 - 12 per group). Tissue mass of dissected white adipose tissue (WAT) depots after sacrifice in the corresponding Arc (**B**) and LHA (**E**) groups. i, inguinal; e, epididymal; m, mesenteric; r, retroperitoneal; total, summed weight of i, e, m and r WAT depots. Whole body lean mass in the corresponding Arc (**C**) and LHA (**F**) groups. Data are means ± SEM and averaged for all mice from each group examined. $*p \leq 0.05$, $**p \leq 0.01$, $***p \leq 0.001$ for $AAV\text{-}Cart$ versus $AAV\text{-}GFP$ treatments.

involved in weight regulation, LHA CART reintroduced on an otherwise CART-negative genetic background may modulate body composition by increasing adiposity and decreasing lean body mass. No apparent difference was seen in the weights of major organs between genotypes in either brain area (Fig. S2 A-B). Interestingly, investigation of Cart^cre/+ mice subjected to CART overexpression in either the Arc or the LHA, which showed unaltered body weight (Figure 3A—B), also revealed unchanged adiposity (Fig. S2 C-F) and lean mass (Fig. S2 G-H) compared to AAV-GFP controls.

As part of the body composition analysis, and based on the known link between CART and bone remodeling [16,46], effects of chronic CART introduction specifically into CART neurons in the Arc or LHA on bone parameters were also examined. Interestingly, neither introduction of CART into the Arc or LHA had any significant effect on both whole body BMD and BMC for either Cart^cre/cre (Fig. S3 A-D) or Cart^cre/+ (Fig. S3 E-H) mice. The unchanged bone mass phenotype suggests that CART neurons in these two hypothalamic regions are not directly involved in bone homeostatic control, while CART in other brain areas may be responsible for the regulation of bone metabolism.

3.4. CART reintroduction in the arc and LHA led to differential effects on food intake and energy expenditure

In order to determine which side of the energy balance equation is responsible for the altered body weight and body composition caused by the selective CART reintroduction into Arc or LHA CART neurons, we next measured spontaneous and fasting-induced food intake in Cart^cre/cre mice. Spontaneous daily food intake under fed conditions was unchanged between Arc^CART and Arc^GFP groups (Figure 5A), excluding food intake alteration as a significant contributing factor to the marked decrease in body weight gain seen in Arc^CART;Cart^cre/cre mice (Figure 3C). In contrast, despite unaltered body weight in Cart^cre/cre mice expressing LHA^CART (Figure 3D), a trend towards higher spontaneous food intake was seen compared with LHA^GFP controls (Figure 5B), which is consistent with the significantly elevated fat mass seen in these mice (Figure 4D—E). Food intake in response to 24-hr fasting was unaffected by replenishing CART expression in Cart^cre/cre mice at either the Arc (Fig. S4 A) or LHA (Fig. S4 B). However, despite similar weight loss from the 24-hr fasting, Arc^CART mice experienced an accelerated weight regain during refeeding compared to Arc^GFP controls (Fig. S4 C). No significant difference in body weight loss and subsequent recovery was seen in the LHA^CART mice (Fig. S4 D).

To also investigate the other component of the energy balance equation - energy expenditure, open-circuit indirect calorimetry was employed. Interestingly, a marked increase in energy expenditure was demonstrated in Arc^CART compared to Arc^GFP Cart^cre/cre mice, both overall and specifically during the light phase (Figure 5C). The elevated energy expenditure may contribute at least in part to the substantial drop in fat mass (Figure 4A—B) and body weight (Figure 3C) observed. On the other hand, LHA^CART mice showed a significant reduction in energy expenditure compared to LHA^GFP controls throughout the entire light cycle (Figure 5D). This reduction in heat dissipation, together with greater food intake (Figure 5B), may account for the increased fat mass in LHA^CART;Cart^cre/cre mice (Figure 4D—E). Prominent nuclei-specific effects of CART reintroduction in CART neurons were also demonstrated in the average energy expenditure over the total 24-hr period between Arc and LHA groups (Figure 5E).

Interestingly, the greater energy expenditure observed in Arc^CART mice was not associated with any significant increase in physical activity, albeit a trend of modest elevation during the light phase (Figure 5F). Similarly, despite notably lower energy expenditure no detectable difference was seen in physical activity in LHA^CART mice compared to

controls (Figure 5G). Correspondingly, the impact of CART administration on overall physical activity was minimal for either the Arc or LHA cohort (Figure 5H), indicating that physical activity had little contribution to the alterations in energy expenditure.

Since a role of CART in thermoregulation has been implicated [20,47], along with the overt changes in energy expenditure seen above, the effects of CART reintroduction on body temperature were examined. Despite heightened energy expenditure, infrared imaging in Arc^CART;Cart^cre/cre mice detected no difference in either whole body temperature, as represented by measurements of the lumbar back area (Figure 5I), or BAT temperature (Figure 5J) indicative of non-shivering thermogenesis [48] when compared to AAV-GFP controls. Interestingly, the pronounced reduction in energy expenditure in LHA^CART;Cart^cre/cre mice is not matched with strong effects on whole body temperature which shows a trend to a reduction relative to controls (Figure 5I). Furthermore, significantly lower BAT temperature (Figure 5J) and BAT weight (Figure 5K) were seen in Cart^cre/cre mice with LHA^CART but not Arc^CART when compared to the respective GFP controls, suggesting an involvement of LHA CART in the regulation of BAT thermogenesis. In addition, as the tail is regarded as a major thermoregulatory organ for heat dissipation [49], tail temperature was also examined and was demonstrated to be significantly increased in LHA^CART but not Arc^CART Cart^cre/cre mice compared with controls (Figure 5L). The elevated tail heat loss possibly contributed to the reduced temperature seen in the whole body (Figure 5I) and the IBAT region (Figure 5J), indicating a potential involvement of CART function in the LHA to the regulation of vasodilation and vasoconstriction [49].

Determination of RER, a measure for fuel source preference, revealed no significant difference between treatments for both Arc (Figure 5M) and LHA (Figure 5N) groups throughout the entire photoperiod as well as when averaged for 24-hr (Figure 5O). However, a modest increase in RER was demonstrated for Arc^CART compared to Arc^GFP Cart^cre/cre mice (Figure 5M), possibly suggesting higher relative preference for carbohydrate over fat as the metabolized fuel, which may be associated with the diminished fat availability (Figure 4A—B).

3.5. CART reintroduction in the arc and LHA induced differential effects on the hypothalamic expression of key peptides in the control of energy homeostasis

To elucidate the neurochemical alterations and the central mechanisms underlying the phenotypes manifested following CART reintroduction into Arc or LHA CART neurons, hypothalamic expression of several neurotransmitters and hormones that are pivotal in the regulation of energy homeostasis were profiled. As CART neurons in the Arc co-express the anorexigenic POMC and are adjacent to the orexigenic NPY neurons [27,32], in situ hybridization was performed to measure the transcript expression of Pomc and Npy in the Arc of Arc^CART mice. Cart^cre/cre mice expressing Arc^CART demonstrated a notable trend to a decrease in Pomc mRNA level (Figure 6A) and significantly reduced Npy expression (Figure 6B) compared to Arc^GFP controls. In contrast, no difference was observed in the Arc mRNA level for either neuropeptide in Arc^CART;Cart^cre/+ mice (Figure 6A—B). Since CART has been implicated as a major regulator of CRH neurons of the hypothalamic-pituitary-adrenal (HPA) axis [50,51], and CART neurons in the Arc are known to innervate CRH neurons in the PVN [30,52], we also investigated the effects of CART targeted to the Arc on Crh mRNA expression in the PVN in either Cart^cre/cre or Cart^cre/+ mice. Interestingly, neither of the genotypes showed any significant impact on Crh mRNA expression (Figure 6C).

In the LHA of both humans and rodents, CART has been reported to have a high level of colocalization with the orexigenic neuropeptide melanin-concentrating hormone (MCH) [36,37]. Orexin, another
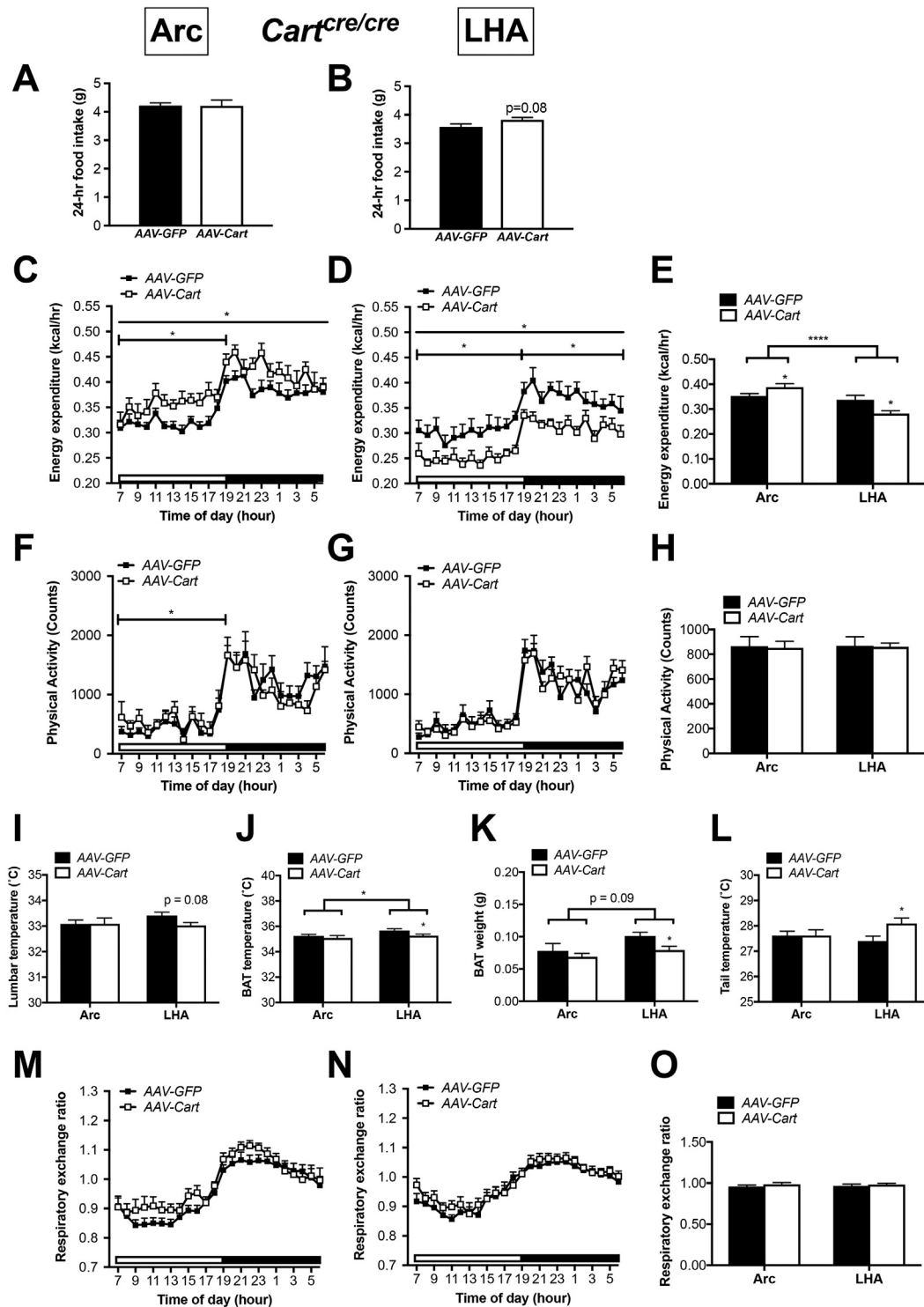
Figure 5: CART reintroduction in *Cart^cre/cre* mice upregulates energy expenditure when targeted in the Arc while downregulating energy expenditure and BAT temperature when introduced into the LHA. Daily spontaneous/basal food intake during fed state in *Cart^cre/cre* mice expressing Arc^CART versus Arc^GFP (**A**) or LHA^CART versus LHA^GFP (**B**) (n = 10 - 12 per group). Indirect calorimetric assessments for the 24-hr time course of energy expenditure (**C**, **D**), physical activity (**F**, **G**) and respiratory exchange ratio (**M**, **N**) to compare Arc^CART against Arc^GFP and LHA^CART against LHA^GFP treatments in *Cart^cre/cre* mice respectively. Corresponding average values for energy expenditure (**E**), physical activity (**H**), and respiratory exchange ratio (**O**) over the total 24-hr period were shown in adjacent bar graphs. Energy expenditure was adjusted for lean mass and compared between groups by analysis of covariance. The adjusted means of energy expenditure were presented at the common lean mass of 22.515 g (Arc) and 21.921 g (LHA) respectively. Open and filled horizontal bars indicate the light and dark photoperiods, respectively. Temperatures of the lumbar back region (**I**), the interscapular brown adipose tissue (IBAT) (**J**), and the tail (**L**) measured by high-sensitivity infrared imaging. (**K**) Dissected BAT mass. Data are means ± SEM and averaged for all mice from each group examined. *$p \leq 0.05$, ****$p \leq 0.0001$ for *AAV-Cart* versus *AAV-GFP* treatments, for comparisons between mice receiving the same treatments at the Arc versus LHA, or for comparisons indicated by horizontal bar.
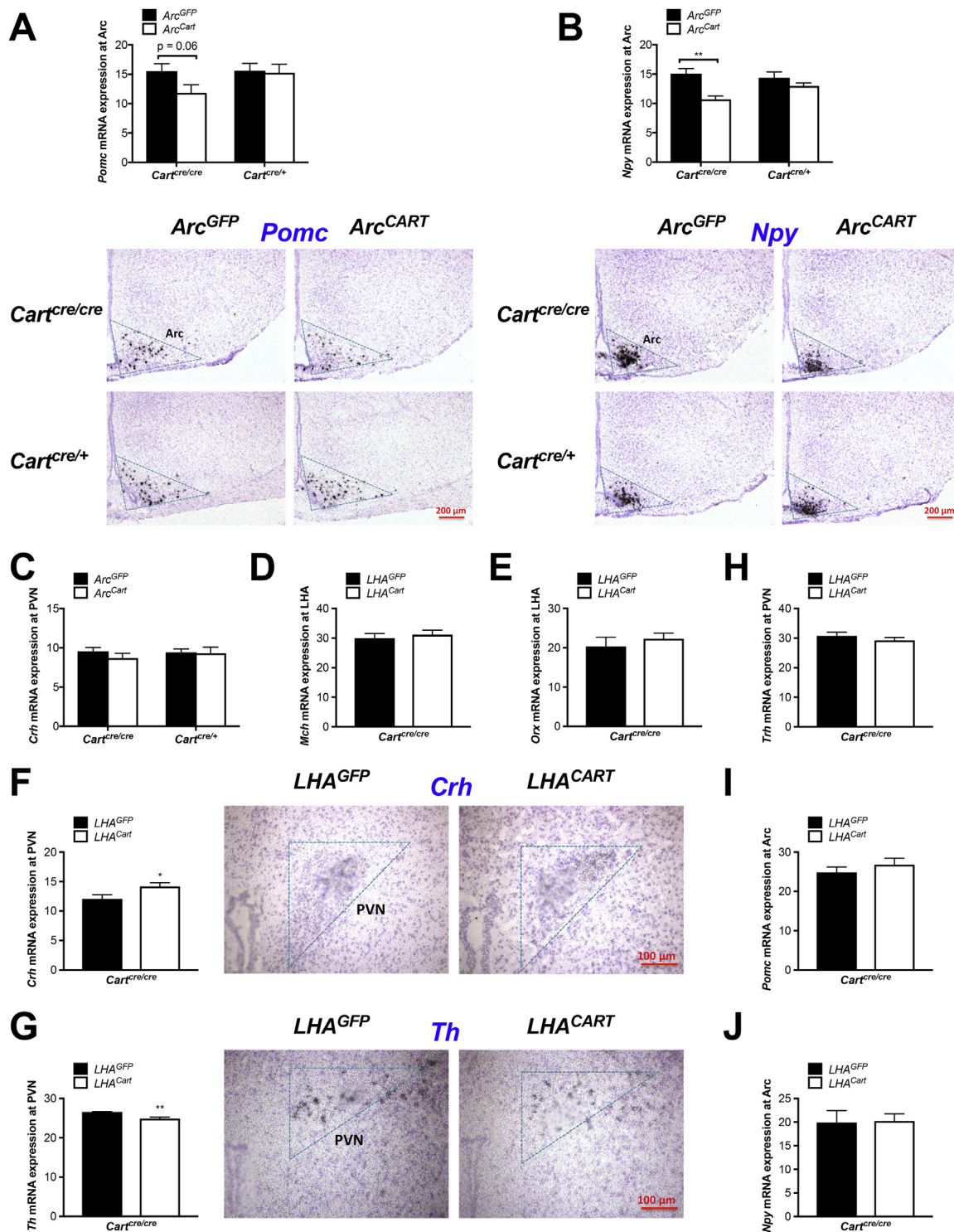
Figure 6: CART neuron-specific CART reintroduction in the Arc and LHA of *Cart^cre/cre* mice differentially impacts mRNA expression of key hypothalamic peptides in the control of energy homeostasis. *In situ* hybridization for *Pomc* (**A**) and *Npy* (**B**) mRNA expression in the Arc and *Crh* (**C**) mRNA expression in the PVN in *Cart^cre/cre* and *Cart^cre/+* mice expressing Arc^CART versus Arc^GFP (n ≥ 5 per group). *In situ* hybridization for *Mch* (**D**) and *Orx* (**E**) mRNA expression in the LHA, for *Crh* (**F**), *Th* (**G**), and *Trh* (**H**) mRNA expression in the PVN, and for *Pomc* (**I**) and *Npy* (**J**) mRNA expression in the Arc in *Cart^cre/cre* mice expressing LHA^CART versus LHA^GFP (n = 5 per group). Bright-field photomicrographs of coronal brain sections showing mRNA expression for *Pomc* (**A**) and *Npy* (**B**) in the Arc, and for *Crh* (**F**) and *Th* (**G**) in the PVN. Scale bar = 200 μm or 100 μm. Hybridization signals are quantified to obtain mean labeling intensity of neurons expressed as percentage coverage of neuronal surface by silver grains (RODs) within the defined areas of interest. PVN, paraventricular nucleus; Arc, arcuate nucleus; *Pomc*, proopiomelanocortin; *Npy*, neuropeptide Y; *Crh*, corticotropin-releasing hormone; *Mch*, melanin-concentrating hormone; *Orx*, orexin; *Th*, tyrosine hydroxylase; *Trh*, thyrotropin-releasing hormone. Data are means ± SEM and averaged for all mice from each group examined. **$p ≤ 0.01$ for *AAV-Cart* versus *AAV-GFP* treatments.

feeding-stimulating peptide, can also be found in the LHA [2,44]. To examine the potential of these two neuropeptides acting together with CART to control feeding and energy homeostasis, mRNA levels of *Mch* and *Orx* were evaluated. Interestingly, CART rescue in the LHA of *Cart^{cre/cre}* mice did not affect the mRNA level of either *Mch* (Figure 6D) or *Orx* (Figure 6E), despite the significant trend towards an increased spontaneous food intake (Figure 5B) seen in these mice. However, LHA^CART;*Cart^{cre/cre}* mice showed significantly higher *Crh* levels (Figure 6F) and a significant decrease in *Th* expression (Figure 6G) in the PVN compared with GFP controls, consistent with the role of these PVN peptides in the regulation of energy expenditure and BAT thermogenesis [43,53]. The reduced *Th* transcript expression was also in line with the potential decrease in vasoconstriction reflected by the greater tail temperature thus heat loss in these mice (Figure 5L). In contrast, the mRNA level of *Trh* in the PVN, another key regulator of the HPA axis with implications in the control of energy balance and thermoregulation [54] was unchanged in LHA^CART;*Cart^{cre/cre}* mice (Figure 6H). Similarly, CART reintroduction into the LHA in *Cart^{cre/cre}* mice had no impact on the expression levels of *Pomc* (Figure 6I) or *Npy* (Figure 6J) in the Arc.

3.6. CART neuron-specific reintroduction of CART in the LHA reduced glucose tolerance and insulin responsiveness

Based on the well-established link between fat metabolism and glucose homeostasis [55] and given the distinctly altered fat content in *Cart^{cre/cre}* mice expressing Arc^CART and LHA^CART, various parameters of glucose metabolism were investigated. Following i.p. glucose challenge, blood glucose levels throughout the 90 min duration were indistinguishable between Arc^CART and Arc^GFP *Cart^{cre/cre}* mice (Figure 7A), as reflected in the unchanged AUCglucose. In contrast, LHA^CART;*Cart^{cre/cre}* mice demonstrated significant higher blood glucose levels compared with GFP controls during the course of IPGTT as shown by the increased AUC (Figure 7B), which suggests reduced glucose tolerance. Interestingly, despite different responses to glucose challenge between the Arc and LHA groups (Figure 7B), serum insulin levels during IPGTT were not different compared to corresponding controls when reintroduced into either the Arc (Figure 7C) or LHA (Figure 7D). Similar to the GTT, insulin responsiveness using the IP-ITT test was not altered between the Arc^CART and Arc^GFP mice displaying unvaried blood glucose levels in response to i.p. insulin (Figure 7E). However, LHA^CART mice with similar initial fasted levels demonstrated significantly higher blood glucose excursion throughout the 90 min period compared to LHA^GFP counterparts (Figure 7F), as reflected by the corresponding, prominent increase in AUCglucose compared to controls (Figure 7F). The reduction in insulin responsiveness may be due to decreased lean mass as well as increased adiposity in these mice, which may thus contribute to the reduced glucose tolerance observed in LHA^CART mice (Figure 7B).

4. DISCUSSION

This study presents the first characterization of energy homeostatic functions of CART specifically expressed in the Arc or LHA in a CART neuron-specific manner, through targeted unilateral AAV-FLEX CART delivery in either the homozygous or heterozygous version of the *Cart-cre* knock-in mice. Intriguingly, in *Cart^{cre/+}* mice with existing endogenous CART expression, CART overproduction in Arc or LHA CART neurons had little effect on any of the body composition and metabolic parameters measured. On the other hand, significant and distinctive changes were demonstrated in *Cart^{cre/cre}* mice subjected to CART neuron-specific reintroduction of CART into the Arc and LHA on

an otherwise CART-deficient background. In *Cart^{cre/cre}* mice, CART selectively targeted to CART neurons in the Arc markedly reduced body weight and fat mass without altering lean mass, whereas CART reintroduction into the LHA led to significant fat mass gain and lean mass loss, resulting in unchanged body weight. Although food consumption was unaltered, Arc^CART;*Cart^{cre/cre}* mice showed an increase in both energy expenditure and physical activity, accompanied by a significant decrease in *Npy* mRNA expression in the Arc, which may have contributed to the observed reduction in adiposity. In comparison, the elevated fat mass in LHA^CART;*Cart^{cre/cre}* mice was associated with greater spontaneous food intake and lower energy expenditure, with significantly reduced *Th* and notably increased *Crh* mRNA levels in the PVN. In line with this, the LHA CART-mediated suppression in energy expenditure was paralleled with a significant drop in BAT temperature and BAT weight, while both parameters remained unchanged in Arc^CART;*Cart^{cre/cre}* counterparts. Interestingly, glucose homeostasis was also differentially regulated in the two groups. While LHA^CART;*Cart^{cre/cre}* mice displayed reduced insulin responsiveness and reduced glucose tolerance, attributed at least in part to the higher fat and lower lean body masses, Arc^CART;*Cart^{cre/cre}* mice, on the other hand, were not influenced in this aspect. These findings demonstrate that CART neurons in the Arc and LHA play differential roles in the control of feeding behavior, body composition, and energy homeostasis.

From existing literature, CART has been classified primarily as anorectic, as summarized from i.c.v. CART studies, as well as global CART knockout rodents [1,20], which showed an increase in body weight gain and adipose mass with unchanged feeding behavior [15,20]. Consistent with this classic view, CART reintroduction into the Arc of otherwise CART-deficient mice leads to reduced body weight and lower fat mass, which is accompanied by increased energy expenditure and physical activity, with unaltered food intake. This confirms the Arc as a crucial hypothalamic site for the anorexigenic potency of CART, since the limited gene dosage from the unilateral CART reintroduction was sufficient to trigger profound catabolic effects. Mechanistically, a substantial decline in the Arc *Npy* level was observed in these mice, which may be responsible, at least in part, for the increased energy expenditure [27], indicating the critical involvement of Arc NPY in CART action in regulating energy homeostasis. As opposed to the catabolic effects displayed in Arc^CART;*Cart^{cre/cre}* mice with unaffected feeding behavior, direct evidence for an orexigenic role of CART is also supported by the LHA^CART-directed elevation in food intake and adiposity under CART-deficient condition. This finding is in line with a prior study where heightened *Cart* expression in the LHA was associated with elevated feeding and body weight [56]. More importantly, the increased adiposity in these mice may be achieved by the alterations in *Th* and *Crh* expression in the PVN, indicating the possible control function of LHA CART neurons on TH and CRH neurons in the PVN. Additionally, the anabolic profile of LHA^CART;*Cart^{cre/cre}* mice comprises a reduction in lean mass, lower energy expenditure, and reduced BAT temperature, suggesting that CART in the LHA regulates energy homeostasis through multiple mechanisms. Furthermore, as the LHA is traditionally described as the hunger center [57], and lesions in the LHA were reported to cause hypophagia and weight loss [58], our results further confirm the significance of CART in the orexigenic activity of the LHA. Moreover, since CART knockout mice showed obesogenic traits [14,15,20], Arc CART activity may exhibit greater baseline potency than CART in the LHA, and is therefore regarded a major contributor to the overall CART system in energy homeostasis. Contrary to our results, previous studies in rodents subjected to intra-Arc or -LHA CART administration showed body weight gain and
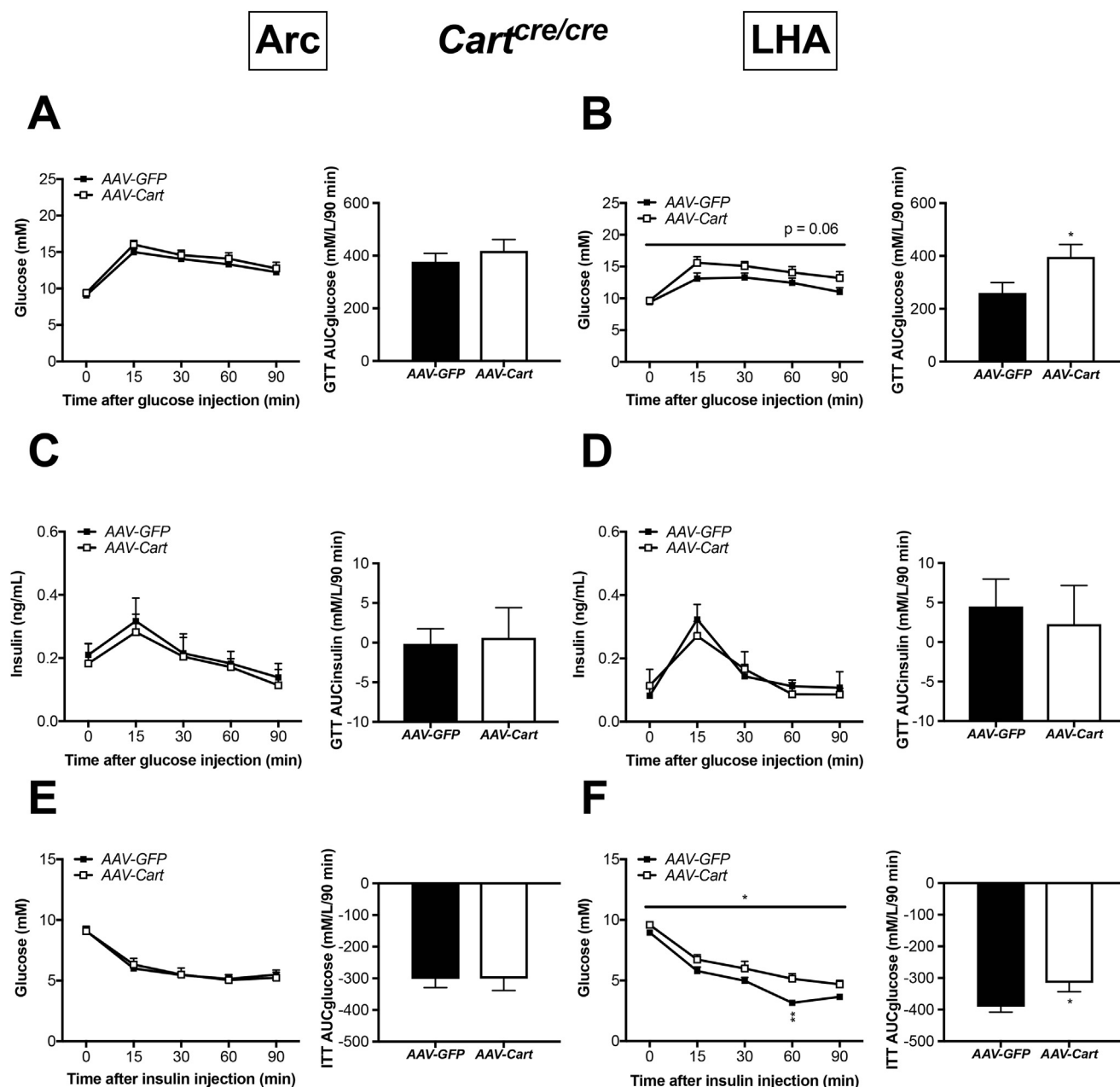
Arc   *Cart*$^{cre/cre}$ LHA

Figure 7: CART neuron-specific rescue of CART expression in the LHA of *Cart*$^{cre/cre}$ mice reduces glucose tolerance and insulin responsiveness. Blood glucose levels during a 90-min intraperitoneal glucose tolerance test (1.0 g/kg body weight) performed in 6-hr fasted *Cart*$^{cre/cre}$ mice expressing Arc^{CART} versus Arc^{GFP} (**A**) or LHA^{CART} versus LHA^{GFP} (**B**) (n = 10 - 12 per group). Adjacent bar graphs showing the area under the glucose concentration curve (AUCglucose) between 0 and 90 min after glucose injection. Corresponding serum insulin levels during the 90-min IPGTT procedure for the Arc (**C**) and LHA (**D**) groups. Adjacent bar graphs showing the area under the insulin concentration curve (AUCinsulin) between 0 and 90 min after glucose injection. Absolute blood glucose levels during a 90-min intraperitoneal insulin tolerance test (0.5 IU/kg body weight) performed in 5-hr fasted *Cart*$^{cre/cre}$ mice expressing Arc^{CART} versus Arc^{GFP} (**E**) or LHA^{CART} versus LHA^{GFP} (**F**). Adjacent bar graphs showing AUCglucose between 0 and 90 min after insulin injection. Data are means ± SEM and averaged for all mice from each group examined. *$p \leq 0.05$, **$p \leq 0.01$ for *AAV-Cart* versus *AAV-GFP* treatments, or for comparisons indicated by horizontal bar.

increased feeding [17—19]. The different responses to CART action are most likely due to the different techniques employed. While the AAV-FLEX strategy employed in this work enables the endogenous processing and synthesis of endogenous CART selectively in CART neurons, previous intra-hypothalamic CART delivery by intranuclear injection or chronic infusion leads to widespread and uncontrolled action of CART peptide in these nuclei and areas. Furthermore, when chemically synthesized CART fragments are used, it is only presumed that these peptides would represent the active form of CART produced

by CART neurons. The representativeness of such methods for replicating physiological CART function may be questionable, as evident in the discrepancy between pharmacological studies [1]. In addition, whilst few studies have identified any impact of CART injection on energy expenditure and physical activity, the two parameters were profoundly and differentially regulated in Arc^{CART} and LHA^{CART} *Cart*$^{cre/cre}$ mice. Further verifying the efficacy of this viral approach for CART expression, this study also provided the first evidence for LHA CART in the regulation of glucose metabolism. However, the reduced

glucose tolerance and insulin responsiveness resulted from CART reintroduction into the LHA could also be secondary to the higher fat and lower lean masses [59] in these mice. Importantly, while hypothalamic CART has been reported to be involved in bone physiology [16,46], our data here show that CART reintroduction into CART neurons in either of the two nuclei had only a minor effect on bone mass, suggesting that other hypothalamic CART neuronal population are more critical for this CART-related control mechanism.

In addition, our study also revealed that overproducing CART in specific CART neurons in the Arc and LHA of $Cart^{cre/+}$ mice does not confer any additive function compared to controls with existing endogenous CART, or enhance any effect seen in the respective $Cart^{cre/cre}$ mice with reintroduced CART expression. The lack of dose response in $Cart^{cre/+}$ mice could either be due to a saturation effect above a certain expression threshold for CART at the particular region or the insufficiency of unilateral CART delivery to generate any detectable physiological shift. Future work involving bilateral targeting of CART may provide additional insights into the validity of this conjecture. Potentially, any effects from the introduced CART in the $Cart^{cre/+}$ mice may also be subject to counterbalancing actions from endogenous CART expressed locally or at other central areas. This further highlights the usefulness of our $Cart^{cre/cre}$ mice as a valuable instrument for determining region-specific CART activity.

In conclusion, via CART neuron-specific reintroduction of CART in CART-deficient mice, the catabolic and anabolic homeostatic influences of CART were demonstrated in the Arc and LHA, respectively. This work supports the notion of an emerging, multifaceted, and nuclei-specific function of CART in appetite control and energy homeostasis regulation. Collectively, our results consolidate the postulation that CART in discrete hypothalamic nuclei performs distinct functions [30–32]. While appetite-stimulating properties were indicated for LHA CART function, Arc CART displayed multiple catabolic impacts. Hence, CART neuronal populations in these two regions may serve as therapeutic entry points for appetite control and body weight maintenance in the treatment of obesity. Future work applying the same design with bilateral CART delivery may facilitate the fine-tuning of CART dosage effects in the presence and absence of endogenous CART. In parallel, comprehensive neurochemical profiling upon CART reintroduction or overexpression in other areas may provide further invaluable insights into the elements and neuronal signaling pathways that interact with the CART system, thereby unraveling the underlying mechanisms linked to CART action in the regulation of feeding and energy homeostasis.

ACKNOWLEDGMENTS

CONFLICT OF INTEREST

No potential conflicts of interest associated with this article were reported and there has been no significant financial support for this work that could have influenced its outcome.

APPENDIX A. SUPPLEMENTARY DATA

Supplementary data related to this article can be found at https://doi.org/10.1016/j.molmet.2017.10.015.

REFERENCES

[1] Lau, J., Herzog, H., 2014. CART in the regulation of appetite and energy homeostasis. Frontiers in Neuroscience 8.

[2] Vrang, N., 2006. Anatomy of hypothalamic CART neurons. Peptides 27:1970–1980.

[3] Koylu, E., Couceyro, P., Lambert, P., Ling, N., DeSouza, E., Kuhar, M., 1997. Immunohistochemical localization of novel CART peptides in rat hypothalamus, pituitary and adrenal gland. J Neuroendocrinol 9:823–833.

[4] Subhedar, N.K., Nakhate, K.T., Upadhya, M.A., Kokare, D.M., 2014. CART in the brain of vertebrates: circuits, functions and evolution. Peptides 54:108–130.

[5] Douglass, J., McKinzie, A., Couceyro, P., 1995. PCR differential display identifies a rat brain mRNA that is transcriptionally regulated by cocaine and amphetamine. The Journal of Neuroscience 15:2471–2481.

[6] Elias, C.F., Lee, C.E., Kelly, J.F., Ahima, R.S., Kuhar, M., Saper, C.B., et al., 2001. Characterization of CART neurons in the rat and human hypothalamus. The Journal of Comparative Neurology 432:1–19.

[7] Menyhért, J., Wittmann, G., Lechan, R.M., Keller, E., Liposits, Z., Fekete, C., 2007. Cocaine- and amphetamine-regulated transcript (CART) is colocalized with the orexigenic neuropeptide y and agouti-related protein and absent from the anorexigenic α-melanocyte-stimulating hormone neurons in the infundibular nucleus of the human hypothalamus. Endocrinology 148:4276–4281.

[8] Thim, L., Kristensen, P., Nielsen, P., Wulff, B., Clausen, J., 1999. Tissue-specific processing of cocaine- and amphetamine-regulated transcript peptides in the rat. Proceedings of the National Academy of Sciences of United States of America 96:2722–2727.

[9] Dominguez, G., 2006. The CART gene: structure and regulation. Peptides 27:1913–1918.

[10] Hubert, G.W., Jones, D.C., Moffett, M.C., Rogge, G., Kuhar, M.J., 2008. CART peptides as modulators of dopamine and psychostimulants and interactions with the mesolimbic dopaminergic system. Biochemical Pharmacology 75:57–62.

[11] Cavalcante, J.C., Cândido, P.L., Sita, L.V., do Nascimento Jr., E.S., Cavalcante, J. d. S., de Oliveira Costa, M.S.M., et al., 2011. Comparative distribution of cocaine- and amphetamine-regulated transcript (CART) in the hypothalamus of the capuchin monkey (Cebus apella) and the common marmoset (Callithrix jacchus). Brain Research 1425:47–61.

[12] Kuhar, M., Yoho, L., 1999. CART peptide analysis by western blotting. Synapse 33:163–171.

[13] Dey, A., Xhu, X., Carroll, R., Turck, C., Stein, J., Steiner, D., 2003. Biological processing of the cocaine and amphetamine-regulated transcript precursors by prohormone convertases, PC2 and PC1/3. Journal of Biological Chemistry 278:15007–15014.

[14] Asnicar, M.A., Smith, D.P., Yang, D.D., Heiman, M.L., Fox, N., Chen, Y.-F., et al., 2001. Absence of cocaine- and amphetamine-regulated transcript results in obesity in mice fed a high caloric diet. Endocrinology 142:4394–4400.

[15] Wierup, N., Richards, W.G., Bannon, A.W., Kuhar, M.J., Ahrén, B., Sundler, F., 2005. CART knock out mice have impaired insulin secretion and glucose intolerance, altered beta cell morphology and increased body weight. Regulatory Peptides 129:203–211.

[16] Elefteriou, F., Ahn, J.D., Takeda, S., Starbuck, M., Yang, X., Liu, X., et al., 2005. Leptin regulation of bone resorption by the sympathetic nervous system and CART. Nature 434:514–520.

[17] Abbott, C.R., Rossi, M., Wren, A.M., Murphy, K.G., Kennedy, A.R., Stanley, S.A., et al., 2001. Evidence of an orexigenic role for cocaine- and amphetamine-regulated transcript after administration into discrete hypothalamic nuclei. Endocrinology 142:3457–3463.

[18] Kong, W., Stanley, S., Gardiner, J., Abbott, C., Murphy, K., Seth, A., et al., 2003. A role for arcuate cocaine and amphetamine-regulated transcript in hyperphagia, thermogenesis, and cold adaptation. The FASEB Journal 17:1688–1690.

[19] Hou, J., Zheng, D.-Z., Zhou, J.-Y., Zhou, S.-W., 2010. Orexigenic effect of cocaine- and amphetamine-regulated transcript (CART) after injection into hypothalamic nuclei in streptozotocin-diabetic rats. Clinical and Experimental Pharmacology and Physiology 37:989—995.

[20] Lau, J., Shi, Y.C., Herzog, H., 2016. Temperature dependence of the control of energy homeostasis requires CART signaling. Neuropeptides.

[21] del Giudice, E.M., Santoro, N., Cirillo, G., D'Urso, L., Di Toro, R., Perrone, L., 2001. Mutational screening of the CART gene in obese children: identifying a mutation (Leu34Phe) associated with reduced resting energy expenditure and cosegregating with obesity phenotype in a large family. Diabetes 50:2157—2160.

[22] Yanik, T., Dominguez, G., Kuhar, M.J., Del Giudice, E.M., Loh, Y.P., 2006. The Leu34Phe ProCART mutation leads to cocaine- and amphetamine-regulated transcript (CART) deficiency: a possible cause for obesity in humans. Endocrinology 147:39—43.

[23] Kristensen, P., Judge, M.E., Thim, L., Ribel, U., Christjansen, K.N., Wulff, B.S., et al., 1998. Hypothalamic CART is a new anorectic peptide regulated by leptin. Nature 393:72—76.

[24] Smith, K.L., Gardiner, J.V., Ward, H.L., Kong, W.M., Murphy, K.G., Martin, N.M., et al., 2008. Overexpression of CART in the PVN increases food intake and weight gain in rats. Obesity 16:2239—2244.

[25] Vicentic, A., Jones, D.C., 2007. The CART (cocaine- and amphetamine-regulated transcript) system in appetite and drug addiction. Journal of Pharmacology and Experimental Therapeutics 320:499—506.

[26] Chu, S.C., Chen, P.N., Ho, Y.J., Yu, C.H., Hsieh, Y.S., Kuo, D.Y., 2015. Both neuropeptide Y knockdown and Y1 receptor inhibition modulate CART-mediated appetite control. Hormones Behavior 67:38—47.

[27] Barsh, G.S., Schwartz, M.W., 2002. Genetic approaches to studying energy balance: perception and integration. Nat Rev Genet 3:589—600.

[28] Zheng, H., Patterson, L.M., Phifer, C.B., Berthoud, H.-R., 2005. Brain stem melanocortinergic modulation of meal size and identification of hypothalamic POMC projections. American Journal of Physiology - Regulatory, Integrative and Comparative Physiology 289:R247—R258.

[29] Elias, C.F., Lee, C., Kelly, J., Aschkenasi, C., Ahima, R.S., Couceyro, P.R., et al., 1998. Leptin activates hypothalamic cart neurons projecting to the spinal cord. Neuron 21:1375—1385.

[30] Fekete, C., Wittmann, G., Liposits, Z., Lechan, R.M., 2004. Origin of cocaine- and amphetamine-regulated transcript (CART)-immunoreactive innervation of the hypothalamic paraventricular nucleus. The Journal of Comparative Neurology 469:340—350.

[31] Elias, C.F., Aschkenasi, C., Lee, C., Kelly, J., Ahima, R.S., Bjorbæk, C., et al., 1999. Leptin differentially regulates NPY and POMC neurons projecting to the lateral hypothalamic area. Neuron 23:775—786.

[32] Cowley, M.A., Smart, J.L., Rubinstein, M., Cerdan, M.G., Diano, S., Horvath, T.L., et al., 2001. Leptin activates anorexigenic POMC neurons through a neural network in the arcuate nucleus. Nature 411:480—484.

[33] Van Vugt, D.A., Lujan, M.E., Froats, M., Krzemien, A., Couceyro, P.R., Reid, R.L., 2006. Effect of fasting on cocaine-amphetamine-regulated transcript, neuropeptide y, and leptin receptor expression in the non-human primate hypothalamus. Neuroendocrinology 84:83—93.

[34] Germano, C.M.R., de Castro, M., Rorato, R., Laguna, M.T.C., Antunes-Rodrigues, J., Elias, C.F., et al., 2007. Time course effects of adrenalectomy and food intake on cocaine- and amphetamine-regulated transcript expression in the hypothalamus. Brain Research 1166:55—64.

[35] Wortley, K.E., Chang, G.-Q., Davydova, Z., Fried, S.K., Leibowitz, S.F., 2004. Cocaine- and amphetamine-regulated transcript in the arcuate nucleus stimulates lipid metabolism to control body fat accrual on a high-fat diet. Regulatory Peptides 117:89—99.

[36] Rossi, M., Choi, S.J., O'Shea, D., Miyoshi, T., Ghatei, M.A., Bloom, S.R., 1997. Melanin-concentrating hormone acutely stimulates feeding, but chronic administration has no effect on body weight. Endocrinology 138:351—355.

[37] Ludwig, D.S., Mountjoy, K.G., Tatro, J.B., Gillette, J.A., Frederich, R.C., Flier, J.S., et al., 1998. Melanin-concentrating hormone: a functional melanocortin antagonist in the hypothalamus. American Journal of Physiology - Endocrinology and Metabolism 274:E627—E633.

[38] Atasoy, D., Betley, J.N., Su, H.H., Sternson, S.M., 2012. Deconstruction of a neural circuit for hunger. Nature 488:172—177.

[39] Rohner-Jeanrenaud, F., Craft, L.S., Bridwell, J., Suter, T.M., Tinsley, F.C., Smiley, D.L., et al., 2002. Chronic central infusion of cocaine- and amphetamine-regulated transcript (CART 55-102): effects on body weight homeostasis in lean and high-fat-fed obese rats. International Journal of Obesity and Related Metabolic Disorders 26:143—149.

[40] Mietzsch, M., Grasse, S., Zurawski, C., Weger, S., Bennett, A., Agbandje-McKenna, M., et al., 2014. OneBac: platform for scalable and high-titer production of adeno-associated virus serotype 1-12 vectors for gene therapy. Human Gene Therapy 25:212—222.

[41] Feil, R., Brocard, J., Mascrez, B., LeMeur, M., Metzger, D., Chambon, P., 1996. Ligand-activated site-specific recombination in mice. Proceedings of the National Academy of Sciences of United States of America 93:10887—10890.

[42] Paxinos, G., Franklin, K.B., 2004. The mouse brain in stereotaxic coordinates, (3rd ed.). San Diego USA: Elsevier Science Publishing Co. Inc.

[43] Shi, Y.-C., Lau, J., Lin, Z., Zhang, H., Zhai, L., Sperk, G., et al., 2013. Arcuate NPY controls sympathetic output and BAT function via a relay of tyrosine hydroxylase neurons in the PVN. Cell Metabolism 17:236—248.

[44] Vrang, N., Tang-Christensen, M., Larsen, P.J., Kristensen, P., 1999. Recombinant CART peptide induces c-Fos expression in central areas involved in control of feeding behaviour. Brain Research 818:499—509.

[45] Lau, J., Farzi, A., Enriquez, R.F., Shi, Y.C., Herzog, H., 2017. GPR88 is a critical regulator of feeding and body composition in mice. Scientific Reports 7:9912.

[46] Gerrits, H., Bakker, N.E., van de Ven-de Laat, C.J., Bourgondien, F.G., Peddemors, C., Litjens, R.H., et al., 2011. Gender-specific increase of bone mass by CART peptide treatment is ovary-dependent. Journal of Bone and Mineral Research 26:2886—2898.

[47] Skibicka, K.P., Alhadeff, A.L., Grill, H.J., 2009. Hindbrain cocaine- and amphetamine-regulated transcript induces hypothermia mediated by GLP-1 receptors. The Journal of Neuroscience 29:6973—6981.

[48] Morrison, Shaun F., Madden, Christopher J., Tupone, D., 2014. Central neural regulation of brown adipose tissue thermogenesis and energy expenditure. Cell Metabolism 19:741—756.

[49] Fischer, A.W., Hoefig, C.S., Abreu-Vieira, G., de Jong, J.M.A., Petrovic, N., Mittag, J., et al., 2016. Leptin raises defended body temperature without activating thermogenesis. Cell Reports 14:1621—1631.

[50] Stanley, S.A., Small, C.J., Murphy, K.G., Rayes, E., Abbott, C.R., Seal, L.J., et al., 2001. Actions of cocaine- and amphetamine-regulated transcript (CART) peptide on regulation of appetite and hypothalamo-pituitary axes in vitro and in vivo in male rats. Brain Research 893:186—194.

[51] Sarkar, S., Wittmann, G.B., Fekete, C., Lechan, R.M., 2004. Central administration of cocaine- and amphetamine-regulated transcript increases phosphorylation of cAMP response element binding protein in corticotropin-releasing hormone-producing neurons but not in prothyrotropin-releasing hormone-producing neurons in the hypothalamic paraventricular nucleus. Brain Research 999:181—192.

[52] Wittmann, G., Liposits, Z., Lechan, R.M., Fekete, C., 2005. Origin of cocaine- and amphetamine-regulated transcript-containing axons innervating hypophysiotropic corticotropin-releasing hormone-synthesizing neurons in the rat. Endocrinology 146:2985—2991.

[53] Richard, D., Lin, Q., Timofeeva, E., 2002. The corticotropin-releasing factor family of peptides and CRF receptors: their roles in the regulation of energy balance. European Journal of Pharmacology 440:189—197.

[54] Lechan, R.M., Fekete, C., 2006. Role of melanocortin signaling in the regulation of the hypothalamic-pituitary-thyroid (HPT) axis. Peptides 27:310—325.

Original Article

[55] Modan, M., Halkin, H., Almog, S., Lusky, A., Eshkol, A., Shefi, M., et al., 1985. Hyperinsulinemia. A link between hypertension obesity and glucose intolerance. Journal of Clinical Investigation 75:809—817.

[56] Yu, Y., South, T., Wang, Q., Huang, X.-F., 2008. Differential expression of hypothalamic CART mRNA in response to body weight change following different dietary interventions. Neurochemistry International 52:1422—1430.

[57] Schwartz, M.W., Woods, S.C., Porte, D., Seeley, R.J., Baskin, D.G., 2000. Central nervous system control of food intake. Nature 404:661—671.

[58] Bellinger, L.L., Bernardis, L.L., 2002. The dorsomedial hypothalamic nucleus and its role in ingestive behavior and body weight regulation: lessons learned from lesioning studies. Physiology Behavior 76:431—442.

[59] Kwankaew, J., Saetung, S., Chanprasertyothin, S., Leelawattana, R., Rattarasarn, C., 2014. Lean mass inversely predicts plasma glucose levels after oral glucose load independent of insulin secretion or insulin sensitivity in glucose intolerance subjects. Endocrine Journal 61:77—83.

118   MOLECULAR METABOLISM 7 (2018) 102—118
www.molecularmetabolism.com